The Momentum Budget of an Intense Midlatitude Squall Line

WILLIAM A. GALLUS, JR. AND RICHARD H. JOHNSON

Department of Atmospheric Science, Colorado State University, Fort Collins, Colorado

(Manuscript received 29 January 1991, in final form 22 July 1991)

ABSTRACT

Rawinsonde data from OK PRE-STORM are used to calculate the momentum budgets of an intense midlatitude squall-line system with a trailing stratiform region. Budgets have been computed at three separate times during the mature through dissipating stages of the squall line using composited data over 3-hour intervals based on 90-minute releases. Budgets have been done in both ground-relative and system-relative reference frames, although system-relative terms are emphasized for comparison with other recent studies. Low-level radar data are used to partition the system into convective line and stratiform regions.

The system contained a strong midlevel mesolow that contributed to rear-to-front pressure gradient acceleration in the vicinity of a rear-inflow jet. The mesolow, located within a larger region of low pressure sloping rearward with height, also led to strong front-to-rear acceleration elsewhere through a majority of the system. Convective-scale effects produced the primary accelerations opposing the pressure gradient. Advections (large during the mature stage) and local momentum tendencies weakened significantly during dissipation. The line-normal vertical momentum flux was generally negative, which might be expected from downgradient arguments applied to presquall vertical wind profiles. However, wind profiles averaged over the convective line region reversed during the mature and dissipating stages so that the calculated flux was countergradient at the budget times, in agreement with other momentum budget studies.

Vertical momentum transport in the along-line direction was weakly positive in the convective line and negative elsewhere. Because the along-line winds generally increased with height at the budget times, the positive transport in the convective line was countergradient, contrary to the downgradient transport often observed for the along-line flow in convective systems. This result is attributed to an alongline asymmetry in the pressure field, namely, a midlevel mesolow in the northern portion of the squall-line system.

1. Introduction

Mesoscale convective systems (MCSs) often significantly affect the larger-scale flow and height fields around them (Sanders and Emanuel 1977; Brown 1979; Fritsch and Maddox 1981; Maddox et al. 1981; Fritsch and Brown 1982; LeMone 1983; Smull and Houze 1987a,b). Unlike isolated convective elements, which simply result in mixing, organized convective systems can lead to an apparent countergradient momentum transport, and accelerations of the flow (Moncrieff 1981; LeMone 1983). The heating and cooling that take place within the systems due primarily to condensation and evaporation often result in the formation of mesohighs at lower and upper levels and a mesolow in midlevels of the troposphere (Fujita 1955; Brown 1979; Maddox et al. 1981). The height perturbations cause accelerations that may be important in the generation or maintenance of strong front-to-rear and rear-inflow jets (Smull and Houze 1987b; Gao et al. 1990). These jets in turn may be important in allowing a convective system to remain active over long time periods by establishing a mechanism for the continuous regeneration of convective elements (Lafore and Moncrieff 1989; Fovell 1991). Convective-scale sources and sinks of momentum appear to be large and a major contributor to accelerations of the larger-scale winds.

One convective system that exhibited both the aforementioned height perturbations and jets moved through the OK PRE-STORM (Oklahoma–Kansas Preliminary Regional Experiment for STORM-Central) domain on 10–11 June 1985 (Augustine and Zipser 1987; Smull and Houze 1987b; Johnson and Hamilton 1988; Rutledge et al. 1988; Zhang and Gao 1989; Zhang et al. 1989; Gao et al. 1990; Johnson et al. 1990; Gallus and Johnson 1991). A dense sounding network was available for this squall-line case, and the compositing of this 90-minute data over 3-hourly time intervals allowed a study of the momentum budget of the system and its evolution from the mature through dissipating stages. Particularly intense height perturbations within the 10–11 June squall line allowed the direct computation of pressure gradients from the rawinsonde data, a technique rarely used since height perturbations are usually insufficiently large to be discerned from inherent errors in the rawinsonde data (Fankhauser 1974).

The effects of momentum transport due to MCSs are still not well understood. Because momentum does

Corresponding author address: William A. Gallus, Jr., Colorado State University, Department of Atmospheric Science, Fort Collins, CO 80523.

not act as a tracer quantity, momentum transport within a convective system is complex. Air is accelerated vertically by buoyancy, and horizontally by the mesoscale pressure forces that may evolve rapidly in the system (LeMone 1983). Coriolis forces can become important since an MCS may last for many hours, and eddy stresses may decelerate the flow. Furthermore, because there are no integral constraints to verify the accuracy of momentum budgets (unlike with heat and moisture budgets) and more importantly, the pressure gradient term is difficult to measure accurately due to a lack of adequate pressure-field data, momentum budgets have not been frequently diagnosed, especially for midlatitude convection. This paper will add to the observational knowledge of momentum transport within midlatitude squall lines.

2. Data analysis and budget equations

For this study, wind and geopotential height data from the PRE-STORM supplemental sounding network were used, in addition to WSR-57 radar data. Composites of the sounding data and low-level radar reflectivity fields were made over 3-hour periods centered at 0300, 0600, and 0730 UTC, using procedures described in Gallus and Johnson (1991, hereafter referred to as GJ). Although the squall line was weakening during the budget times, it was felt that the 3-hour composite interval was brief enough to allow a steady-state assumption. It will later be shown (Figs. 9, 16, and 18) that the local derivative in a reference frame moving with the system was generally small, particularly when averaged over the system, supporting the steady-state assumption. The location of the composited rawinsonde sites and radar echo at the three times can be found in Fig. 1 (from Gallus and Johnson 1991). Compositing decreased the average station spacing from around 150 to 80 km, allowing better resolution of mesoscale features within the broad stratiform portion of the system. Features within the ~40-km–wide leading convective line, however, could not be fully resolved. (Since inadequate resolution of small-scale features in the convective line is a problem common to all rawinsonde-based budget studies, however, comparisons will still be made between the convective line region of this case and some earlier cases.) Wind and height data from one bogus sounding were used in the momentum budgets. This sounding was placed in a data-sparse area of the presquall environment at 0600 UTC (shown as the circle well ahead of the system in Fig. 1b), using data averaged from two other presquall sites in order to reduce aliasing of convective line features into that area. Data from the composited rawinsondes were gridded onto a 0.5° by 0.5° grid using a Barnes objective analysis scheme (Barnes 1964). Details of the procedure are also described in GJ. Finite differences were used for both horizontal and vertical derivatives, with an interval of 1.0° in the horizontal and 50 mb in the vertical.

Vertical p velocities used in the budgets were calculated from the kinematic technique using the mass continuity equation. Adjustments were made (from O'Brien 1970) so that ω vanished at 125 mb, which was the height of the highest tropopause in the region. A sloped lower boundary was assumed for the ω calculations, and is described in GJ.

The u and v momentum budget equations used (from Stevens 1979, modified as in Gao et al. 1990 for a system-relative coordinate system) are

$$\bar{X} \equiv \frac{D\bar{u}}{Dt} + (\bar{u} - C)\frac{\partial \bar{u}}{\partial x} + \bar{v}\frac{\partial \bar{u}}{\partial y} + \bar{\omega}\frac{\partial \bar{u}}{\partial p} + \frac{\partial \bar{\phi}}{\partial x} - f\bar{v}$$

$$= -\nabla\cdot(\overline{\mathbf{V}'u'}) - \frac{\partial}{\partial p}(\overline{\omega' u'}) \quad (1)$$

$$\bar{Y} \equiv \frac{D\bar{v}}{Dt} + (\bar{u} - C)\frac{\partial \bar{v}}{\partial x} + \bar{v}\frac{\partial \bar{v}}{\partial y} + \bar{\omega}\frac{\partial \bar{v}}{\partial p} + \frac{\partial \bar{\phi}}{\partial y} + f\bar{u}$$

$$= -\nabla\cdot(\overline{\mathbf{V}'v'}) - \frac{\partial}{\partial p}(\overline{\omega' v'}) \quad (2)$$

where the system-relative local tendency is expressed as $D/Dt = \partial/\partial t + C\partial/\partial x$, and $\bar{X}$ and $\bar{Y}$ are residuals representing the source of momentum due to subgrid-scale effects in the line-normal (x) and along-line (y) directions, respectively. The system propagation speed, C, normal to the line was 16.0 m s^{-1} at 0300 UTC, 13.0 m s^{-1} at 0600 UTC, and 14.0 m s^{-1} at 0730 UTC (see GJ for details concerning the determination of system motion). The system-relative coordinate system allows comparison of the local tendencies and horizontal advections with those terms in the numerical simulation of this case by Gao et al. (1990). The equations given are essentially similar to those found in Gao et al. (since C is approximately constant), with their velocity U equivalent to $\bar{u} - C$. Earlier momentum budgets were generally determined relative to the ground (Sanders and Emanuel 1977; LeMone 1983; Smull and Houze 1987a), but concentrated on terms that are not affected by the change of reference frame, so that comparisons are still possible. Overbars in the equations represent averages of the rawinsonde wind and height data over 50 km × 50 km areas centered at each grid point. Primes denote deviations from those averages.

Because of strong front-to-rear flow through the leading convective line on 10–11 June, both the horizontal and vertical convergences of the eddy momentum fluxes may have been important in producing accelerations of the flow. If so, then the determination of the vertical fluxes $\overline{w'u'}$ and $\overline{w'v'}$ from vertical integration of (1) and (2), as is frequently done, may be subject to errors. Recent studies using Doppler radar data give conflicting results as to the relative importance of the horizontal convergence term. Smull and Houze

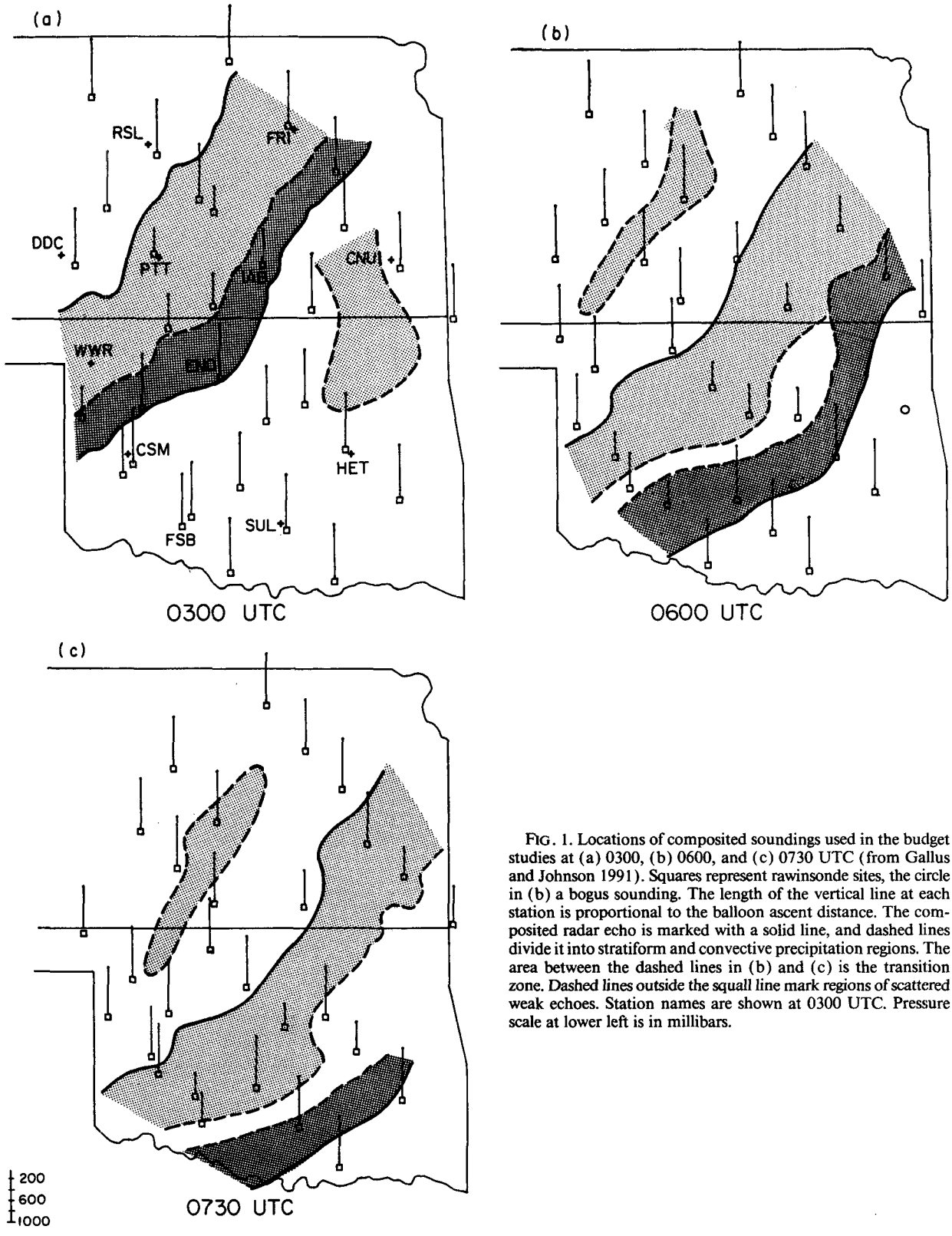

FIG. 1. Locations of composited soundings used in the budget studies at (a) 0300, (b) 0600, and (c) 0730 UTC (from Gallus and Johnson 1991). Squares represent rawinsonde sites, the circle in (b) a bogus sounding. The length of the vertical line at each station is proportional to the balloon ascent distance. The composited radar echo is marked with a solid line, and dashed lines divide it into stratiform and convective precipitation regions. The area between the dashed lines in (b) and (c) is the transition zone. Dashed lines outside the squall line mark regions of scattered weak echoes. Station names are shown at 0300 UTC. Pressure scale at lower left is in millibars.

(1987a) found the term to be generally small in the midlatitude squall line they studied, but Matejka and LeMone (1990) showed that horizontal convergence was comparable to other budget terms at certain levels in a different case. A numerical simulation of this case showed that although the horizontal flux itself was often large, the horizontal flux divergence was about two orders of magnitude smaller than other terms in the momentum budget (Zhang 1991, personal communication). Because the budget contribution due to the horizontal convergence of the eddy momentum flux cannot be isolated and determined from the sounding data, and the evidence given suggests that it may be relatively small, it will be neglected in (1) and (2), so that the equations can be vertically integrated to determine the vertical eddy fluxes. Thus, this study will be consistent with previous rawinsonde-based momentum budget studies.

The rawinsonde height measurements used in this study are calculated hydrostatically, using a virtual temperature that does not take liquid water loading into account. The virtual temperature that should be used in the hypsometric equation to provide accurate height measurements in regions of high radar reflectivity is defined as

$$T_v^* \equiv \frac{T_v}{1 + q_l}, \tag{3}$$

where q_l is the liquid-water mixing ratio, and T_v is the virtual temperature taking only specific humidity into account. The presence of liquid water within a column causes a 1000–500-mb thickness change of roughly 6 m per 1 kg kg^{-1} of liquid-water mixing ratio. Sanders and Emanuel (1977) have determined that the neglect of liquid water in a column in calculating height measurements can cause errors in the pressure field as large as 1 or 2 mb in regions of heavy precipitation. Within the stratiform rain region of convective systems, liquid water loading should not be significant since radar reflectivities are generally low. For the 10–11 June case, it appeared that errors at midlevels due to liquid water loading would be on the order of a few meters, rather small compared to the observed height perturbations. Within the convective line region, however, the failure to include liquid-water mixing ratios when calculating heights can cause errors as large as 10 or 20 m at midlevels. This region, though, is already more susceptible to error since it is not adequately resolved by rawinsonde data. In addition to errors due to liquid water loading, other errors in the height measurements can occur in intense convection due to dynamic processes that make the heights nonhydrostatic. Therefore, momentum budget results for the convective line region are less reliable than results for the stratiform region, but some qualitative comparisons may still be made with convective line region budgets of other cases since the aforementioned problems are common to all rawinsonde-based studies.

3. Mesoscale structure

The squall line began before 2100 UTC 10 June as "broken line" convection (Bluestein and Jain 1985) over southwestern Kansas and the Oklahoma Panhandle ahead of a cold front, and later grew to include a transition zone (defined by Smull and Houze 1985) and broad stratiform rain region as it passed through the PRE-STORM network. The convective line reached peak intensity around 0300 UTC, the first composite time considered in this study. After 0300 UTC, the low-level radar reflectivities in the leading line decreased, while the stratiform region expanded in size through 0600 UTC, the second budget study time. After 0600 UTC, all portions of the system began to weaken markedly, and the final budget study was done during this time at 0730 UTC. A detailed description of the squall-line history and synoptic setting can be found in Johnson and Hamilton (1988).

a. Mesoscale flow

The horizontal and vertical velocities within the 10–11 June squall line have been discussed in detail in GJ; therefore, only brief mention of the flow will be made here. The system-relative airflow normal to the squall line consisted of a series of three well-defined mesoscale jets. These jets can be seen in Fig. 2 (GJ). [In Fig. 2 and all vertical cross sections to be shown, the data presented are the along-line averages of a variable using all the grid points within 50-km–wide strips centered at given distances (see figures) away from the leading edge of the radar echo (analogous to Ogura and Liou 1980). Horizontal cross sections of the components of the line-normal momentum budget show a high degree of two-dimensionality, so that this averaging gives an accurate picture of the general structure of the system.] Briefly, a strong front-to-rear jet ascended from low levels at the leading edge of the system to around 200 mb at its rear, and this jet weakened as the system dissipated. A rear-inflow jet intensified between 0300 and 0600 UTC (Figs. 2a,b) and remained relatively strong through 0730 UTC (Fig. 2c), extending to within 1 km of the surface at the leading edge of the system. Another front-to-rear jet, the result of an overturning downdraft fed by divergence beneath the stratiform region, maintained its intensity over time at the lowest levels beneath the rear-inflow jet.

The along-line component of the winds is shown in Fig. 3 (GJ). Southwesterly flow was dominant except in the vicinity of the rear-inflow jet where northeasterly flow existed. At high levels, the magnitudes of the southwesterly component of the flow were slightly greater than those of the line-normal component, but the flow did weaken as the system dissipated. Peak

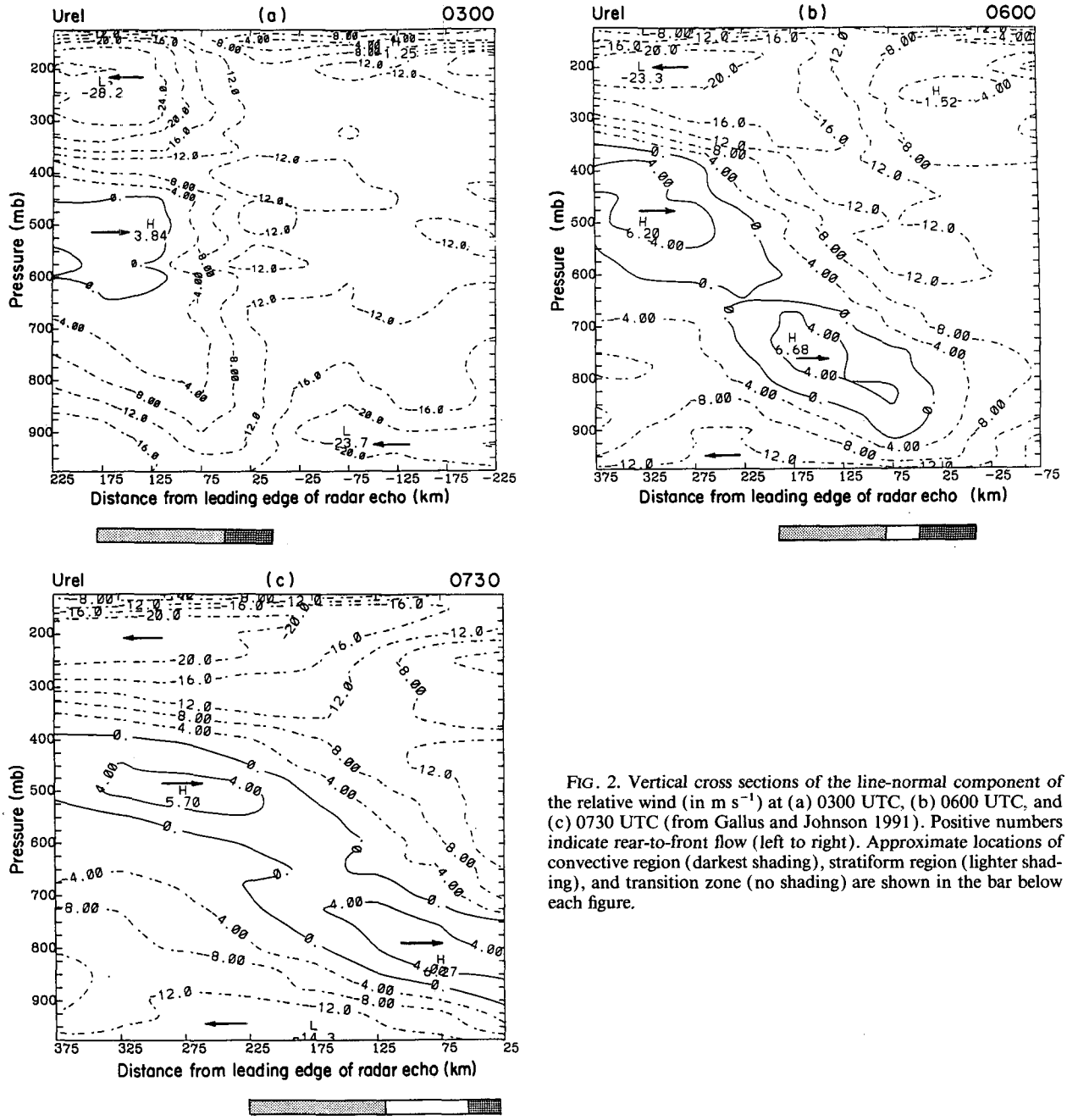

FIG. 2. Vertical cross sections of the line-normal component of the relative wind (in m s^{-1}) at (a) 0300 UTC, (b) 0600 UTC, and (c) 0730 UTC (from Gallus and Johnson 1991). Positive numbers indicate rear-to-front flow (left to right). Approximate locations of convective region (darkest shading), stratiform region (lighter shading), and transition zone (no shading) are shown in the bar below each figure.

speeds decreased from 36 m s^{-1} at 0300 UTC (Fig. 3a) to 28 m s^{-1} at 0600 UTC (Fig. 3b) to just over 20 m s^{-1} at 0730 UTC (Fig. 3c). The low-level northeasterly flow intensified during the dissipation of the squall line.

Vertical p velocities can be seen in Fig. 4. The main features are 1) a region of upward motion in the leading convective line and 2) a region of descent to its rear in the stratiform region. Upward motion near the leading edge of the system weakened and the axes of strongest upward and downward motion became increasingly tilted as the system dissipated. At 0300 UTC (Fig. 4a) peak upward motion was occurring near 400 mb. At 0600 UTC (Fig. 4b) two peaks existed, with one near 600 mb in the convective line and another near 400 mb over the transition zone. At 0730 UTC (Fig. 4c), the maximum upward motion was at 300 mb over the transition zone and front part of the stratiform region. Downward motion occupied an increasing area over time in the stratiform rain region, although max-

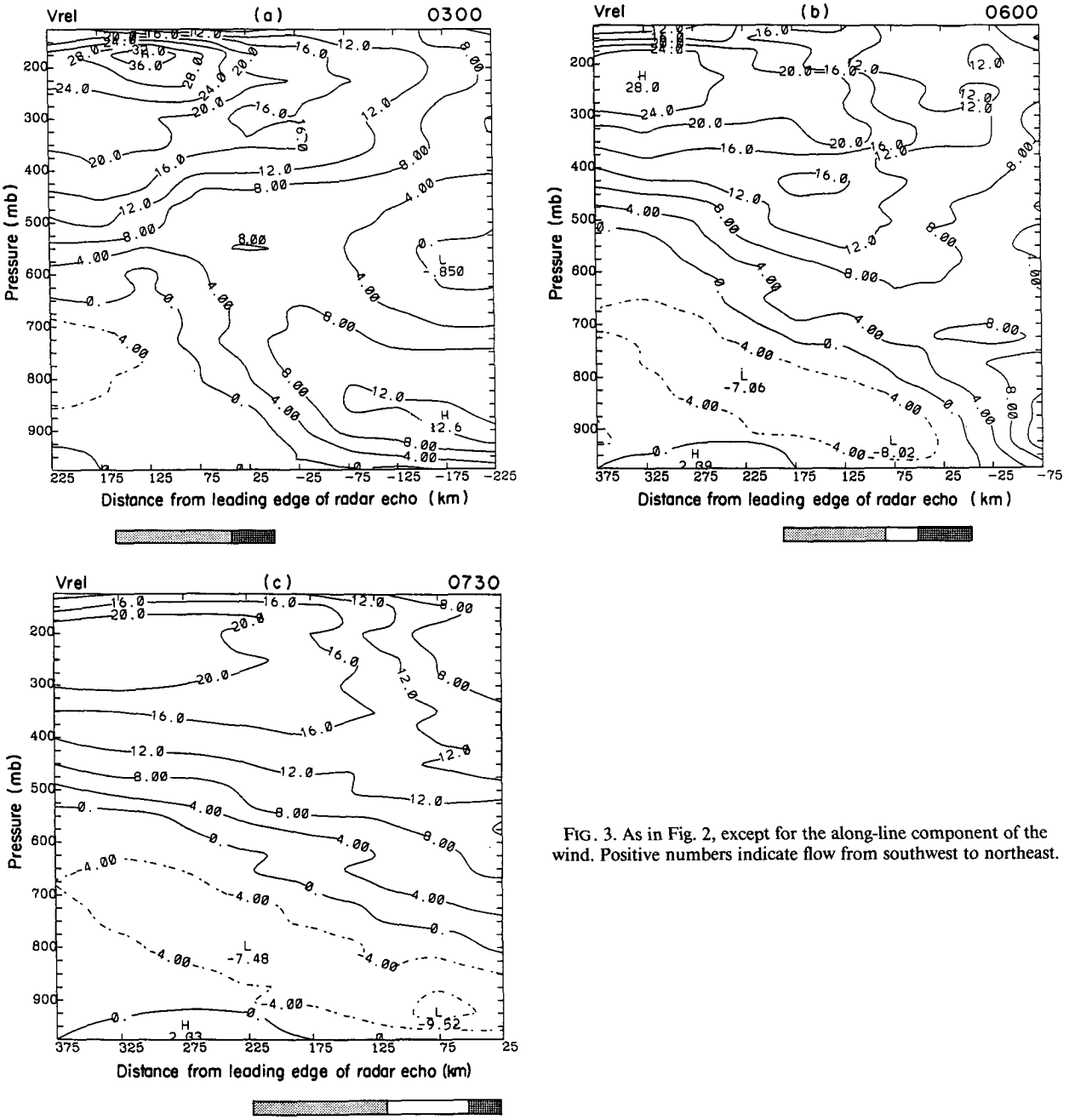

FIG. 3. As in Fig. 2, except for the along-line component of the wind. Positive numbers indicate flow from southwest to northeast.

imum amplitude occurred at 0600 UTC when the stratiform rain was most intense (inferred from radar reflectivities). The peak descent (particularly evident at 0600 UTC) near the melting level (about 625 mb) agrees with the Doppler results of Rutledge et al. (1988) for this case.

b. Geopotential heights

The 10–11 June squall line was associated with a pronounced midlevel trough or mesolow (Sanders and Emanuel 1977; Brown 1979; Menard and Fritsch 1989). This mesolow remained evident throughout the dissipating stages of the system, and can be seen in the height analyses at 700 mb (Fig. 5). The low may have developed prior to the squall-line initiation, as argued by Zhang et al. (1989). Sounding data from times prior to the initial time used in this budget study indicate its presence at 0130 UTC with a possible closed mesolow near Pratt, Kansas. Analyses at earlier times are more ambiguous since the feature had not entered the me-

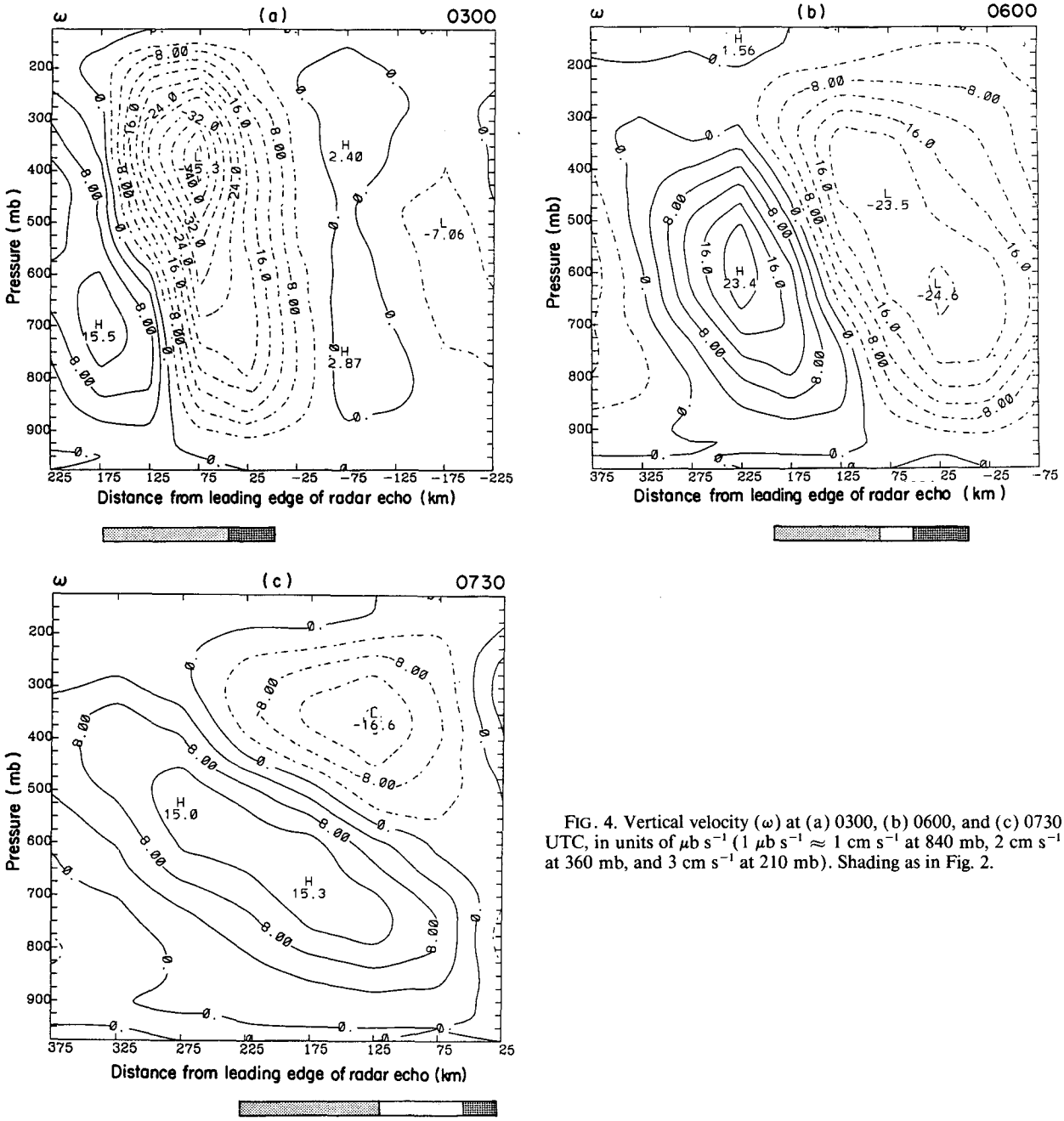

FIG. 4. Vertical velocity (ω) at (a) 0300, (b) 0600, and (c) 0730 UTC, in units of $\mu b\ s^{-1}$ ($1\ \mu b\ s^{-1} \approx 1\ cm\ s^{-1}$ at 840 mb, $2\ cm\ s^{-1}$ at 360 mb, and $3\ cm\ s^{-1}$ at 210 mb). Shading as in Fig. 2.

sonetwork. At 0300 UTC (Fig. 5a) the center of lowest pressure was located in southern Kansas within the stratiform rain area. At 0600 UTC (Fig. 5b) a pressure trough in the stratiform region extended the length of the system, and it was still evident at 0730 UTC (Fig. 5c). The position of the mesolow and trough axis well inside the back edge of the radar echo agrees with the results obtained by Matejka (1989), who used the Doppler retrieval method to determine the height perturbations within the stratiform region of this system. This mesolow is hydrostatically induced (GJ), the result of latent heat release aloft within the stratiform-region anvil cloud above evaporative cooling and melting (Brown 1979; Leary and Houze 1979) taking place within the stratiform rain below cloud base. A distinct and separate, yet also hydrostatically induced, low has been found near the rear of the convective portion of a squall-line system by LeMone (1983) for

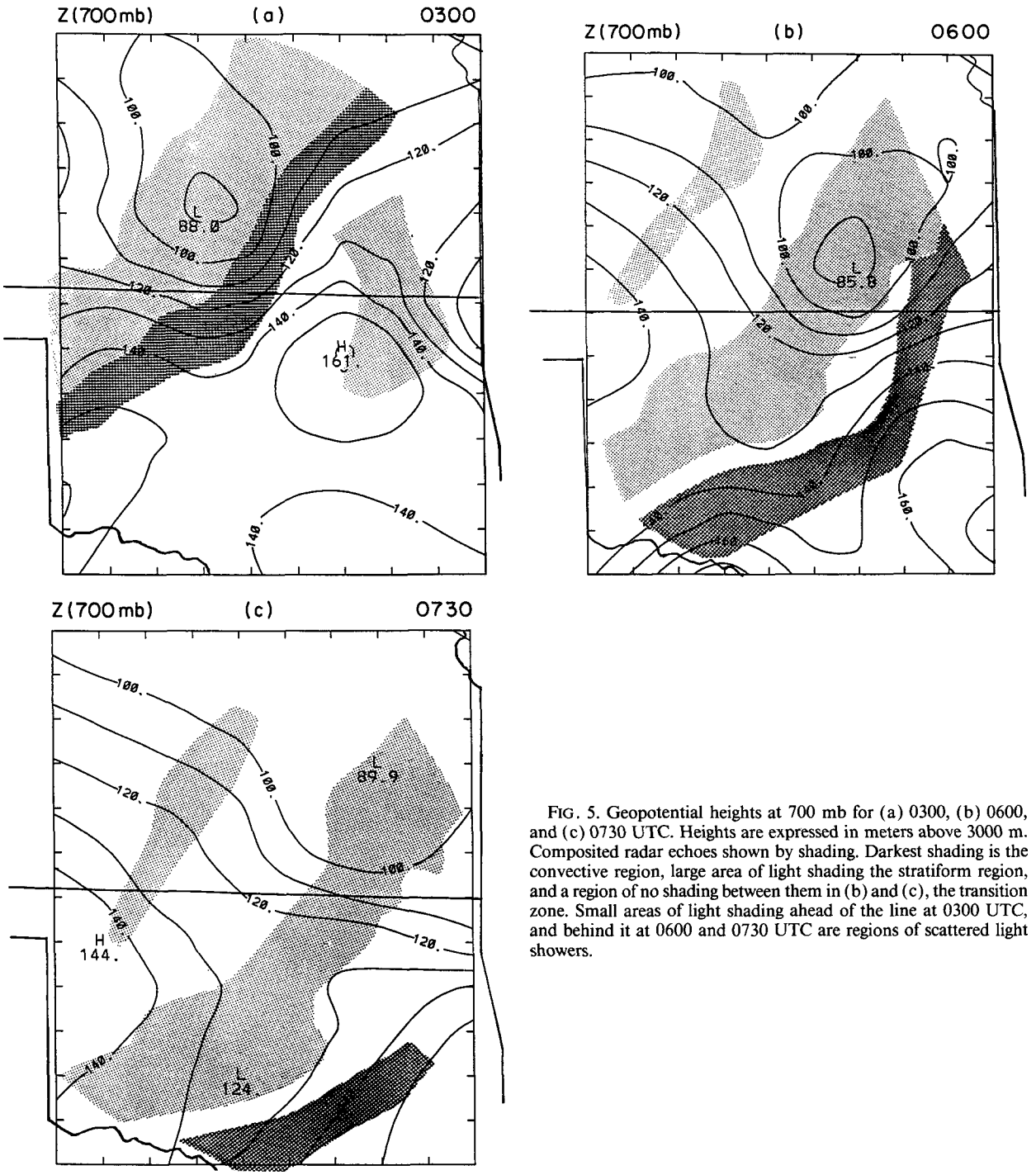

FIG. 5. Geopotential heights at 700 mb for (a) 0300, (b) 0600, and (c) 0730 UTC. Heights are expressed in meters above 3000 m. Composited radar echoes shown by shading. Darkest shading is the convective region, large area of light shading the stratiform region, and a region of no shading between them in (b) and (c), the transition zone. Small areas of light shading ahead of the line at 0300 UTC, and behind it at 0600 and 0730 UTC are regions of scattered light showers.

a GATE system, occurring immediately under warm convective updrafts. If such a low exists in this system, it is too small to resolve with the rawinsonde height data used in this study.

Because a reliable synoptic-scale analysis of heights was not available for the budget times studied, height perturbations were computed from differences between heights at individual grid points at a particular pressure level and the average height of all grid points at that latitude across the PRE-STORM domain in order to determine the vertical structure of the mesoscale pressure field within the squall line. The results at 0300,

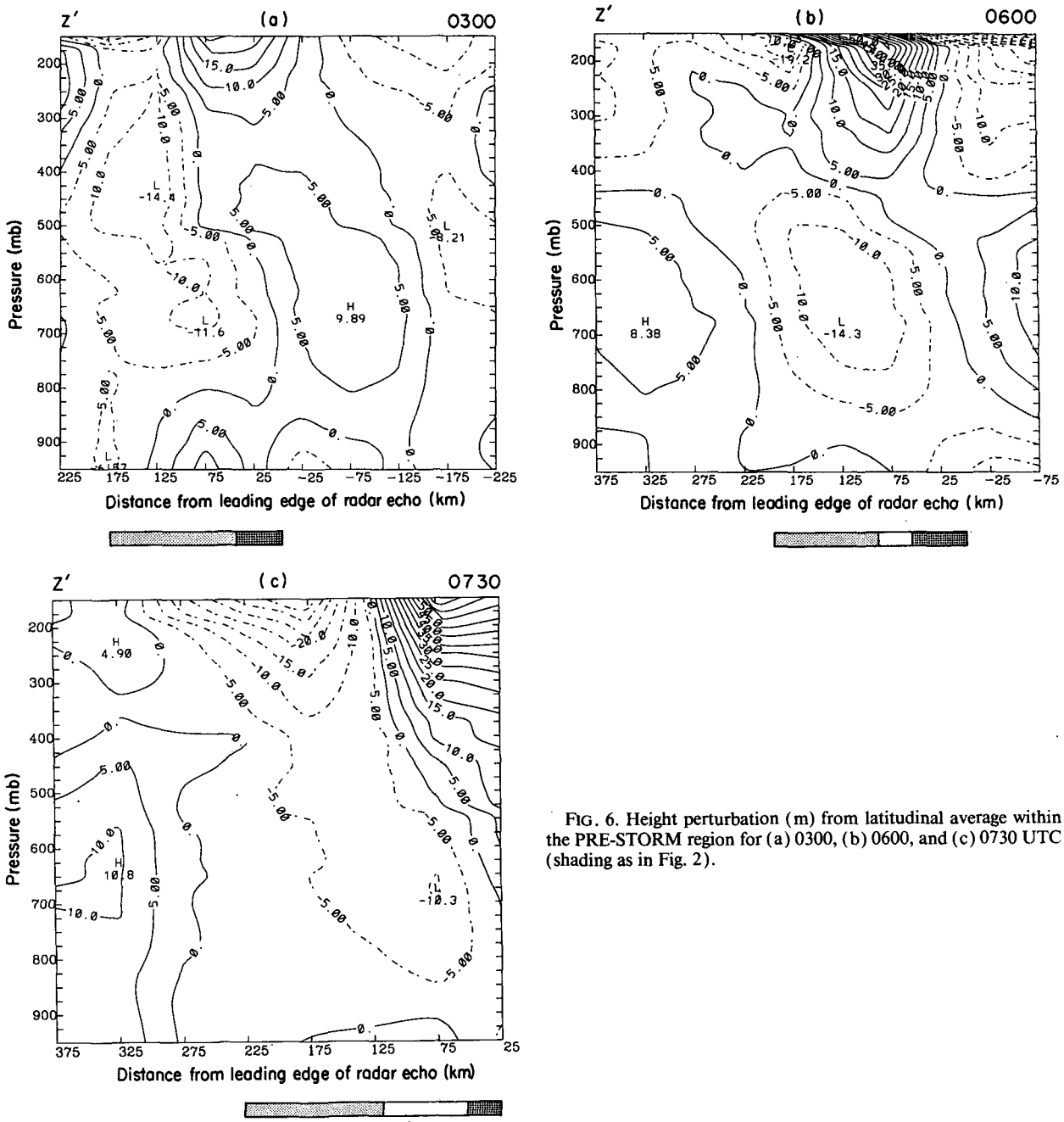

FIG. 6. Height perturbation (m) from latitudinal average within the PRE-STORM region for (a) 0300, (b) 0600, and (c) 0730 UTC (shading as in Fig. 2).

0600, and 0730 UTC are presented in Fig. 6. Caution must be exercised in comparing vertical variations in the perturbations in Fig. 6, since the height deviations are computed at individual levels and are independent of each other. At 0300 UTC (Fig. 6a) a mesolow is evident within the stratiform region extending from 800 mb to near 200 mb and sloping toward the rear of the system. A relative mesohigh existed at midlevels just ahead of the convective line and also extended rearward with its maximum intensity near the tropopause over the system. (Both the relative mesohighs at midlevels and the negative height perturbations at high levels over the stratiform region at all three budget times are most likely a result of requiring the perturbations to average to zero at constant latitudes over the PRE-STORM domain. It is likely that the midlevel mesolow was more pronounced, and a broader perturbation mesohigh existed at high levels all across the squall-

line system.) At low levels, a wake low, mesohigh, and presquall mesolow can be seen, as discussed in Johnson and Hamilton (1988).

At 0600 UTC (Fig. 6b) the low-level features were not as pronounced, probably a result of the weakening of the system. A strong midlevel mesolow continued over the system with peak intensity over the stratiform region. Relative midlevel mesohighs existed ahead of and behind the system. A very intense mesohigh could be seen near the tropopause over the squall line. The magnitude of the mesohigh may be exaggerated in our analyses (also at 0730 UTC; Fig. 6c) due to the ascent of one sounding through an updraft core, but widespread divergence aloft (figure not shown) qualitatively supports the presence of this feature (Maddox et al. 1981; Wetzel et al. 1983). By 0730 UTC (Fig. 6c) some of the same features could still be seen, although the convective line was leaving the data network. In particular, a mesohigh trailed the system at midlevels with the mesolow most intense over the transition zone. An intense upper-level mesohigh continued over the front portion of the system. Although a direct comparison cannot be made with the numerical simulation of this case by Zhang and Gao (1989) and Gao et al. (1990) because of different methods of determining height perturbations, the low-high-low pattern at low levels, the midlevel mesolow with relative mesohighs ahead of and behind it, and the upper-level mesohigh determined from the rawinsonde data (Fig. 6) can also be inferred from the perturbation heights obtained in that simulation.

4. Momentum budget of the line-normal flow

a. Temporal and spatial variations

Equation (1) expresses the balance of forces affecting the component of the horizontal velocity normal to the squall line. Figures 7–12 detail variations of these forces (per unit mass), or accelerations, in the vertical across the squall line. The horizontal pressure gradient force, or generation term, was calculated from the gridpoint height data and can be seen in Fig. 7. At 0300 UTC (Fig. 7a), a large region of front-to-rear acceleration was acting near the front of the system, extending to the tropopause. Peak accelerations exceeded 10 m s^{-1} h^{-1}. Near the rear of the system, some rear-to-front acceleration acted in the vicinity of the rear-inflow jet. Stronger rear-to-front acceleration was acting in the convective line near the surface where a tight pressure gradient existed between the presquall mesolow and mesohigh. Gao et al. (1990) have linked both the region of strong rear-to-front acceleration near the surface at 0300 UTC and the rear-to-front acceleration at midlevels farther to the rear at the back of the system with the expansion of the rear-inflow jet during the mature stage of this system. Their model simulation found rear-to-front accelerations due to the pressure gradient of over 25 m s^{-1} h^{-1} in the surface layer at 0300 UTC. The two features are not as intense in our analyses and the regions of positive acceleration are not connected. However, the rear-inflow jet did appear to have two speed maxima at later times (0600 UTC, Fig. 2b; 0730 UTC, Fig. 2c), which may reflect the two separate maxima in the rear-to-front pressure gradient.

At 0600 and 0730 UTC (Figs. 7b,c) strong front-to-rear pressure gradient accelerations continued to act at low- and midlevels over the convective region and at high levels over the stratiform area. At 0600 UTC (Fig. 7b) rear-to-front acceleration was concentrated near the rear-inflow jet with peak intensities exceeding 3 m s^{-1} h^{-1}, as at 0300 UTC, but the area covered by rear-to-front acceleration broadened and intensities weakened slightly by 0730 UTC (Fig. 7c), when the system was dissipating rapidly. The large region influenced by rear-to-front pressure gradient acceleration at 0730 UTC may account for the persistence of the rear-inflow jet at this time, in spite of the rapid weakening of the squall line. Gao et al. (1990) have found in their model simulation of this system that the generation term was the most important term contributing to both the rear-to-front acceleration that sustained the rear-inflow jet, and the ascending front-to-rear jet ahead of it. The pressure gradient acceleration at high levels at 0600 and 0730 UTC (Figs. 7b,c) appears to be adversely affected by the anomalous heights from one sounding, but qualitatively is correct. Although no rear-to-front outflow was found ahead of the system at high levels by rawinsondes at these times (Figs. 2b,c), the front-to-rear flow around 250 mb decreased significantly between 0300 and 0600 UTC, which may be evidence that some rear-to-front pressure gradient acceleration was acting nonetheless, as shown in Fig. 7.

The acceleration caused by the Coriolis force was generally from rear to front at all times, except at low levels within the stratiform region and to the rear of the system (Fig. 8). This pattern reflects a larger-scale short wave passing through the region, evidenced by a northerly flow at low levels and the turning of the wind from a more northwesterly direction to southwesterly at mid-to-upper levels moving from west to east across the PRE-STORM domain (Johnson and Hamilton 1988). The magnitudes of this acceleration were rather small with peak values found at high levels, weakening gradually from over 10 m s^{-1} h^{-1} at 0300 (Fig. 8a) to 8 m s^{-1} h^{-1} at 0600 (Fig. 8b) and roughly 7 m s^{-1} h^{-1} by 0730 UTC (Fig. 8c). The Coriolis acceleration generally opposed the acceleration due to the pressure gradient, a result also found by Stevens (1979) for a GATE case.

The system-relative local tendency term (Fig. 9) and horizontal and vertical advections (Figs. 10 and 11) were computed from gridded wind data, with the tendency term (Du/Dt) computed as a finite difference

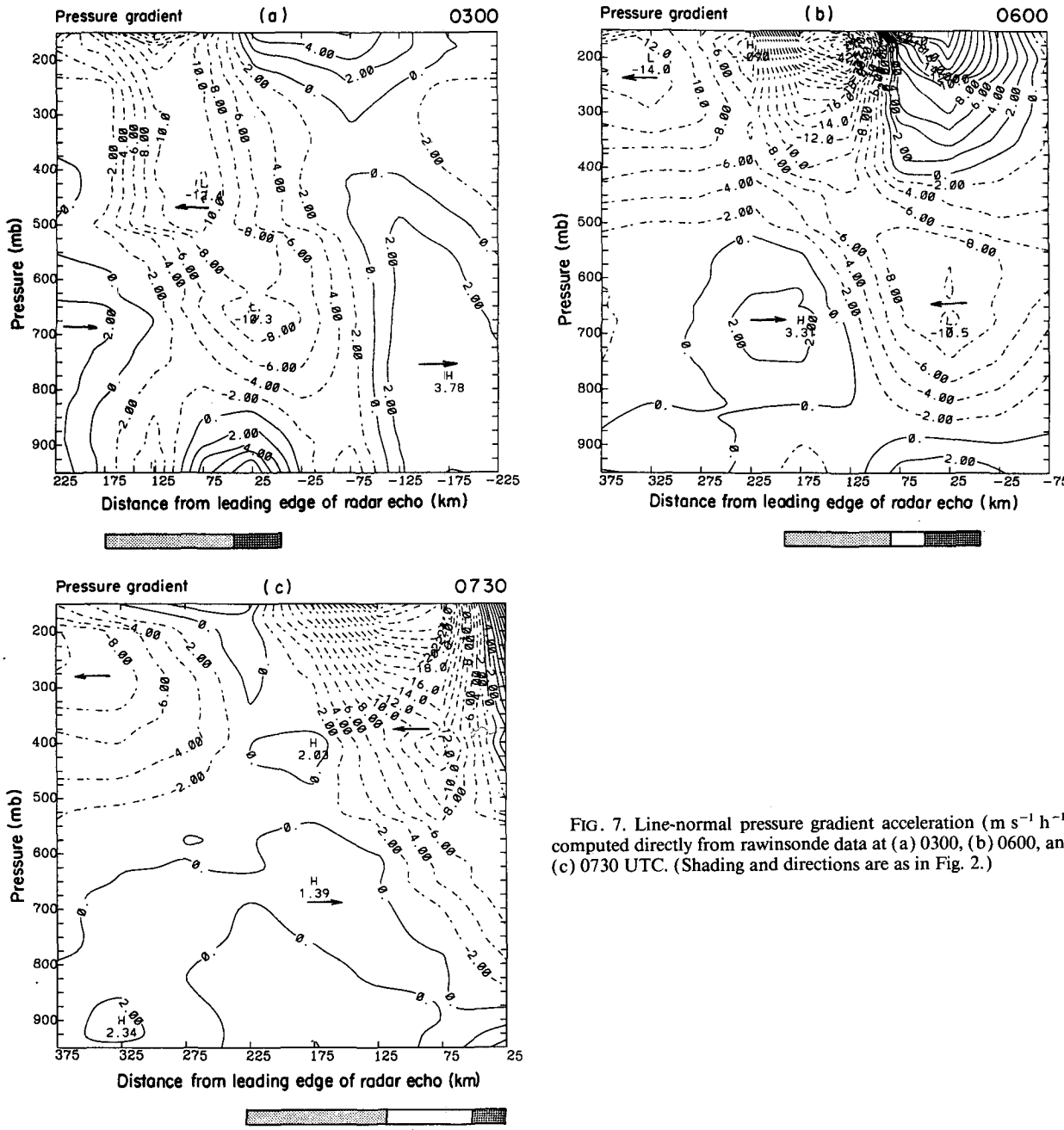

FIG. 7. Line-normal pressure gradient acceleration (m s^{-1} h^{-1}) computed directly from rawinsonde data at (a) 0300, (b) 0600, and (c) 0730 UTC. (Shading and directions are as in Fig. 2.)

over the 3-hour time interval. Noncomposited gridded wind data were obtained at the start and end times of the 3-hour composite interval. At 0300 UTC (Fig. 9a) local tendencies were generally positive at low levels with one maximum just ahead of the leading edge and another near the rear of the stratiform region. Strong rear-to-front tendencies could also be found in the 500–600-mb layer at the rear of the system. This was the region of the rear-inflow jet, and the local tendencies support the observation that this jet remained strong or even intensified at this stage of the system's life cycle. Positive values were also occurring at high levels over the stratiform region, with negative values just to its rear. Negative tendencies dominated midlevels within the squall line, probably the result of some weak intensification of the mesolow when averaged over the length of the squall line (cf. Fig. 5). The observed tendencies at high levels may indicate that, although negative acceleration was acting at distances greater than 175 km to the rear of the leading edge, possibly accel-

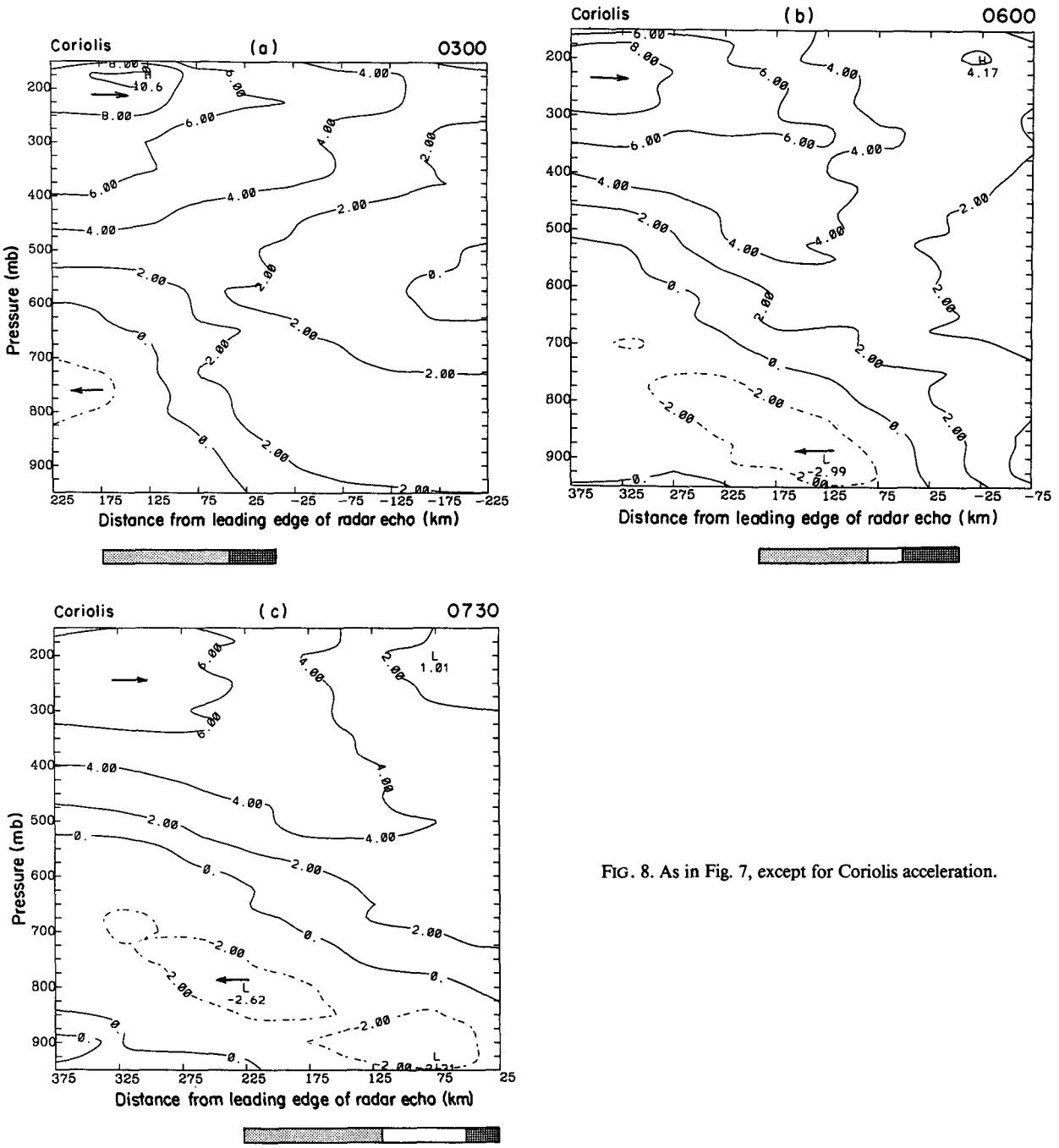

FIG. 8. As in Fig. 7, except for Coriolis acceleration.

erating the rearward transport of hydrometeors within the rear of the stratiform region to broaden the anvil at this time, rearward transport within the forward part of the anvil was diminishing. This weakening is consistent with the eventual weakening of rain rates in that region.

By 0600 UTC (Fig. 9b) local tendencies had weakened markedly. At low levels, positive tendencies could still be found ahead of the system, but were generally weak elsewhere. Negative tendencies were occurring around 700 mb within the stratiform region, and around 450 mb to the rear of the system. Both regions were within or at the leading flank of the rear-inflow jet, as in Gao et al. (1990). This would indicate a weakening of the rear-to-front flow. Likewise, positive tendencies, which were somewhat concentrated in a

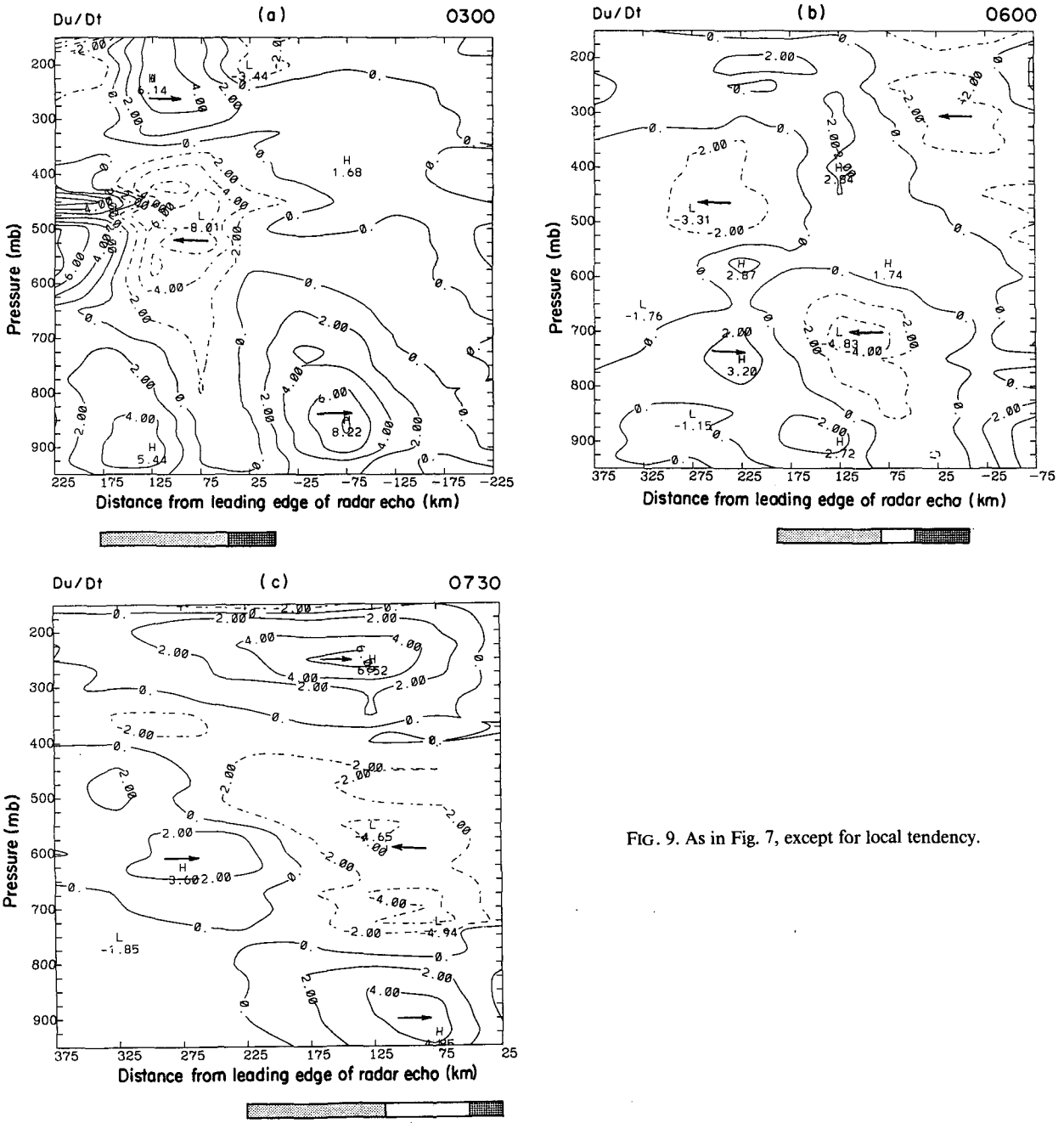

FIG. 9. As in Fig. 7, except for local tendency.

zone ahead of the negative tendencies, show a weakening of the front-to-rear ascending flow. Both of these results were also found by Gao et al. (1990).

At 0730 UC (Fig. 9c) three main bands of differing tendencies dominated the region. Positive tendencies were occurring at low levels below and within the lower part of the rear-inflow jet, as were negative tendencies throughout midlevels and positive tendencies at most high levels. The positive tendencies in the vicinity of the forward part of the rear-inflow jet may indicate a lowering and restrengthening of the nose of that jet. Maximum velocities in the jet were nearly as large at 0730 UTC as they had been at 0600 UTC (see Fig. 2), and the lower maxima had advanced and descended toward the convective line. In addition, the jet appeared to expand slightly in area by 0730 UTC. The rear-to-front tendencies aloft agree with observations that the radar echo began breaking up rapidly at this time, and rain rates decreased about 30% in the stratiform region (GJ). The position of the lower bands appears to agree

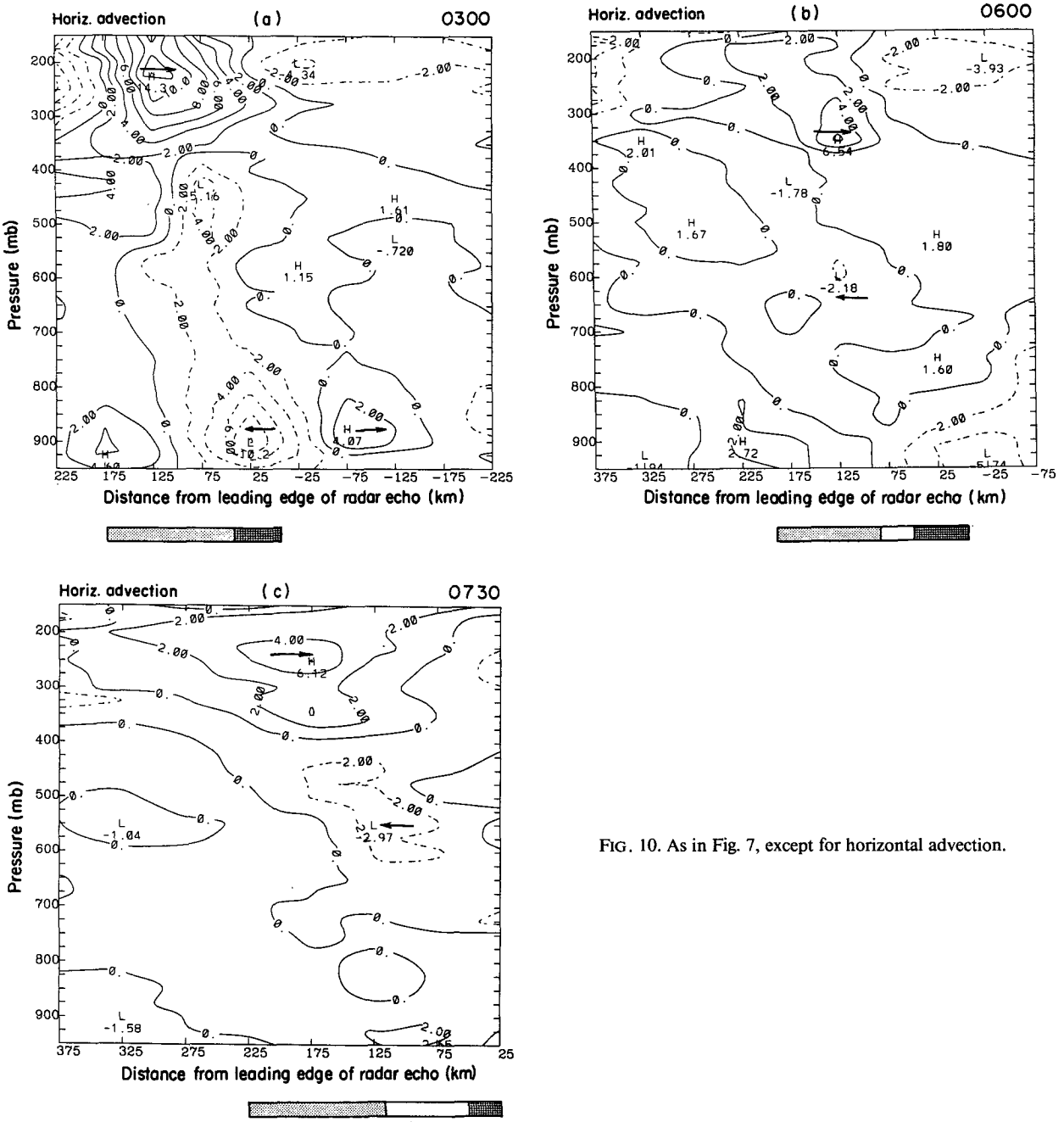

FIG. 10. As in Fig. 7, except for horizontal advection.

with the simulation results at 0600 UTC (the last time shown) by Gao et al. (1990).

Horizontal advections can be seen in Fig. 10. At 0300 (Fig. 10a) these advections were from rear to front in a band extending from low levels ahead of the leading edge to high levels in the stratiform region, where peak positive values were over 14 m s^{-1} h^{-1}. Front-to-rear horizontal advection was prevalent below 400 mb within both the convective line and stratiform region. Peak values occurred around 900 mb in the convective line. These patterns agree well with Gao et al. (1990). Horizontal advections became much weaker at 0600 and 0730 UTC (Figs. 10b,c). At 0600 UTC (Fig. 10b) the most intense positive advections occurred around 350 mb over the front portion of the stratiform region. Weak negative advections were occurring generally just above and ahead of the rear-inflow jet, as in Gao et al., but the magnitudes were far

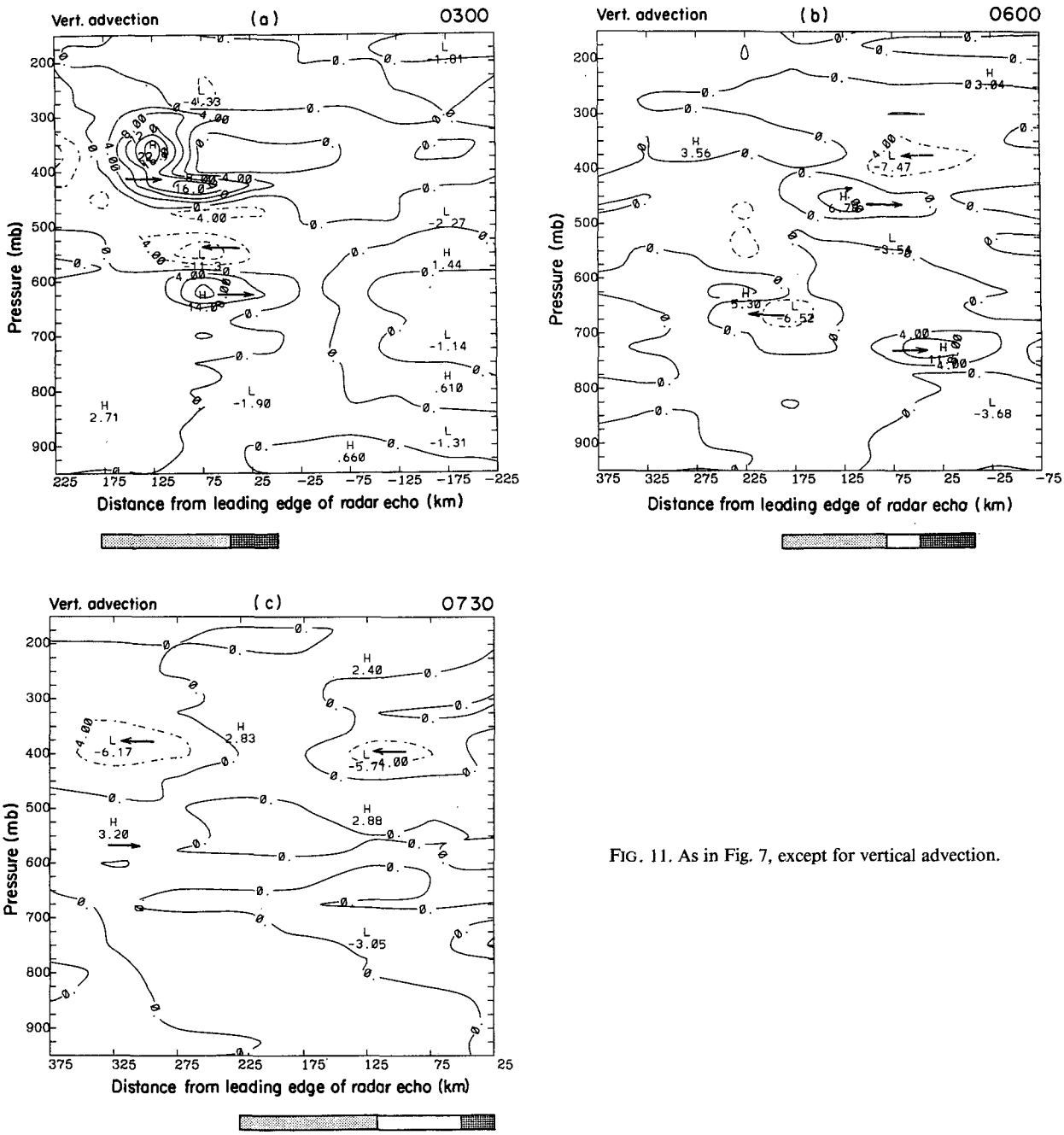

FIG. 11. As in Fig. 7, except for vertical advection.

weaker. At 0730 UTC (Fig. 10c) horizontal advections continued to be weak, and the greatest rear-to-front advections were still at high levels over the stratiform region.

Vertical advections are shown in Fig. 11. Because small-scale jets may have been present within the intense convection, this field is rather variable. The vertical advections were most intense at 0300 UTC (Fig. 11a) when the convection was still active within the squall line. Two levels in particular within the convective system were experiencing strong rear-to-front advection, one near 600 mb and the other in the 300–450-mb layer. There is a similar double-peaked pattern in the numerical simulation of this case by Gao et al. (1990), although the intervening negative tendencies were not diagnosed in their simulation. At 0600 UTC (Fig. 11b) the vertical advections had weakened markedly. Again, two small regions exhibited relatively

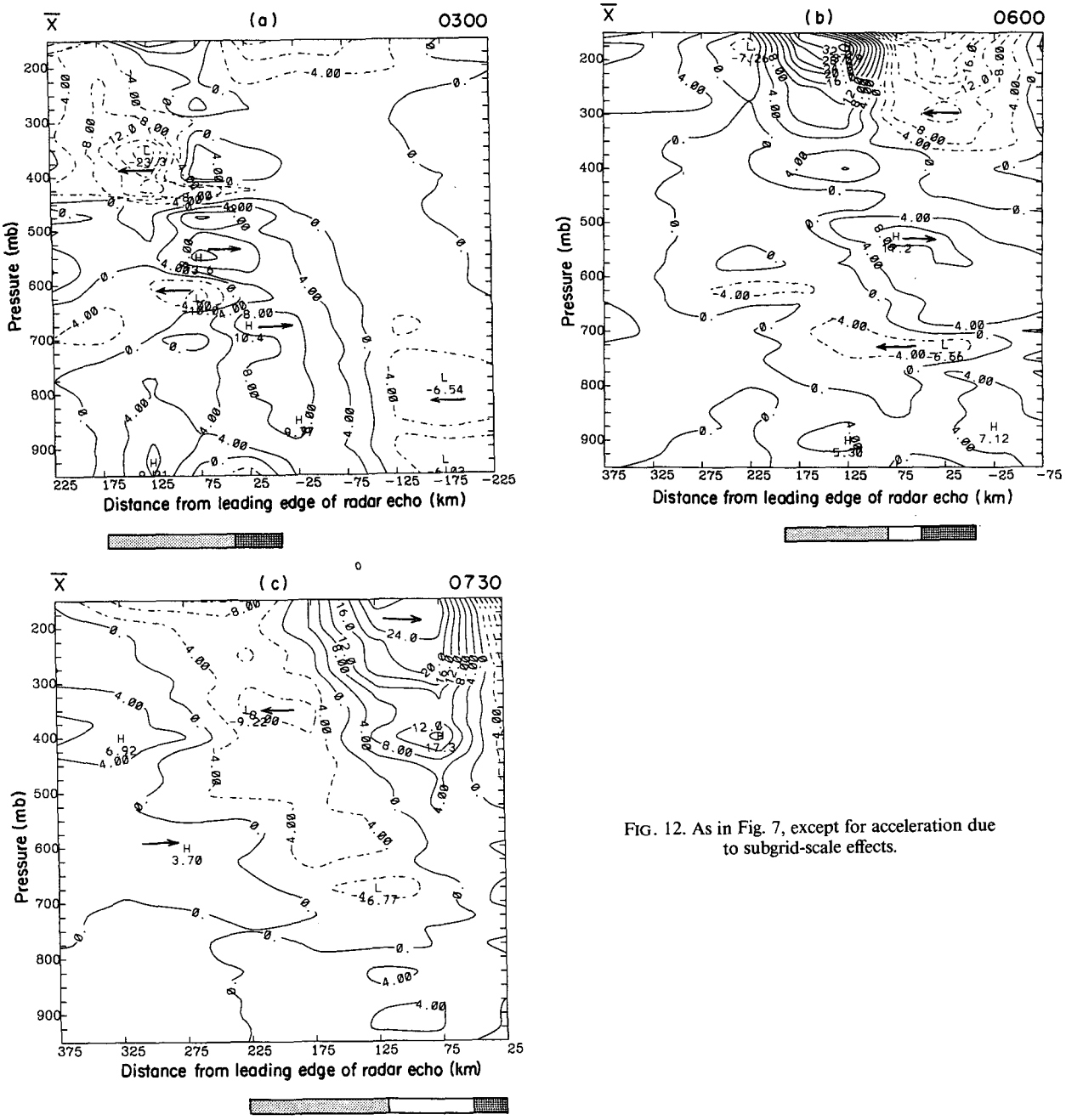

FIG. 12. As in Fig. 7, except for acceleration due to subgrid-scale effects.

strong rear-to-front acceleration, with one around 700 mb and the other around 450 mb. Further weakening occurred by 0730 UTC (Fig. 11c) at which time the field of vertical advection was rather disorganized.

The difference between the total observed acceleration (the horizontal and vertical advections subtracted from the local tendency) and the pressure gradient and Coriolis accelerations, assuming errors in the data are relatively small, is an indication of subgrid-scale effects on the momentum budget ($\bar{X}$). These subgrid-scale sources and sinks of momentum can be seen in Fig. 12. At 0300 UTC (Fig. 12a), the pressure gradient and Coriolis force generally opposed each other everywhere (Figs. 7a and 8a), so that the field of $\bar{X}$ was similar to the sum of the tendency and advection terms, particularly the vertical advection (Fig. 11a) above 700 mb (where these advections were intense). Generally, positive values of $\bar{X}$ existed at low levels with negative values aloft. At later times (0600, Fig. 12b; 0730, Fig. 12c), when the local tendencies and advections were

weaker, the subgrid-scale effects appeared to oppose the pressure gradient accelerations, as in Gao et al. (1990). The main subgrid-scale sources of momentum at all times (positive acceleration) were found at low levels in the convective line region, sloping rearward with height (Fig. 12). It appears that this strong positive acceleration at low levels was at least partly responsible for the observed maxima in the local tendency found around 900 mb (Fig. 9a,b). It can be inferred from the line-normal winds (Fig. 2), vertical velocities (Fig. 4), and subgrid-scale acceleration (Figs. 12a,b) that this was a region of intensely negative vertical momentum flux divergence, probably due to the entrainment of ambient-momentum air by convective clouds. This entrainment would lead to positive acceleration.

Sinks of momentum (negative acceleration) generally occurred at mid- and high levels toward the rear of the system (Fig. 12), especially at 0300 and 0730 UTC (Figs. 12a,c). Negative acceleration acted in some areas in the vicinity of the rear-inflow jet [just below and ahead of the jet ~600 mb at 0300 UTC (Fig. 12a), 650–800 mb, ahead of the jet axis at 0600 UTC (Fig. 12b), and throughout the jet at 0730 UTC (Fig. 12c)]. This front-to-rear acceleration was most pronounced just ahead of the axis of the rear-inflow jet at 0600 UTC (Fig. 12b), when it exceeded 5 m s^{-1} h^{-1}. A similar maximum in front-to-rear acceleration from turbulent forces was found in the study by Gao et al. (1990). This acceleration may be a result of turbulent mixing within the intense shear layer just above the axis of the jet. Evidence of such mixing has been reported as Kelvin–Helmholtz waves in the single-Doppler radar analyses of Houze et al. (1989). The magnitudes of the subgrid-scale stresses were often comparable to those of the Coriolis and pressure gradient acceleration, agreeing with results from other cases studied by Sanders and Emanuel (1977), LeMone (1983), and Smull and Houze (1987a).

At high levels, above about 400 mb, at 0600 and 0730 UTC (Figs. 12b,c), unreasonably large values of $\bar{X}$ were due, in part, to the distorted height field resulting from a rawinsonde ascending in an updraft core. Some gravity waves may also have caused turbulence in the outflow layer. In this environment, turbulent forces should be largest in areas where vigorous convection is occurring (Sanders and Emanuel 1977), and this observation is one check on the validity of solving for the turbulent stresses, or convergence of the eddy momentum fluxes, as a residual in the momentum budget. As can be seen in Fig. 12, the subgrid-scale sources and sinks were generally larger in the convective system than outside it, and their magnitudes decreased as the convection weakened.

At 0300 UTC (Fig. 12a), the subgrid-scale effects tended to increase the negative vertical wind shear in the 700–400-mb layer in the convective line, with little influence below 700 mb (cf. Fig. 2a), but at the later times, the subgrid-scale momentum transport, operating on a wind profile already changed markedly by the convective system, tended to decrease the negative shear from 700 to roughly 550 mb and decrease the positive shear in the convective line at most levels above 550 mb (Fig. 2b). In the stratiform region at all times, subgrid-scale effects were a source of momentum at low levels (generally below 700–800 mb) and a sink in mid- to high levels (except above ~500 mb at 0600 UTC, but the data in this region may be contaminated in part by the updraft-core sounding). These effects therefore decreased the positive shear beneath the rear-inflow jet (Fig. 2). Above the jet, subgrid-scale effects increased the negative shear at 0300 UTC (intense convective activity may have been aliased into the stratiform region at this time), but decreased the negative shear at 0600 UTC. The effects were weak and variable at 0730 UTC (Fig. 2c).

b. Area-averaged force balances

Earlier momentum budget studies have dealt primarily with the balance of forces within the convective line regions of mesoscale convective systems (Sanders and Emanuel 1977; LeMone 1983), and have sought to explain the effects of the convection on the local wind shear. The evolution of ground-relative u and v can be seen in Figs. 13 and 14 (for system-relative speeds, subtract C from u). Shown are a presquall average taken from six rawinsondes located at least 100 km ahead of the leading edge of the convective system around 0130 UTC (Figs. 13a and 14a), and averages over the convective line regions at 0300 UTC (Figs. 13b and 14b), and again at 0600 UTC (Figs. 13c and 14c). Ahead of the system, the line-normal velocity generally increased with height (positive shear), except below 925 mb, and in a layer near 200 mb (Fig. 13a). However, at 0300 UTC, u varied irregularly within the convective line (Fig. 13b), and by 0600 UTC, the u component of the wind shear had reversed below 400 mb from what it was prior to the arrival of the system (Fig. 13c). The presquall along-line winds were directed from southwest to northeast with lower- and upper-level maxima at 775–875 mb and 175 mb, respectively, and a distinct minimum in midlevels (Fig. 14a). At 0300 UTC, within the convective line, the lower-level maximum had disappeared and strong positive shear was present (Fig. 14b). Winds below 450 mb did not change appreciably between 0300 and 0600 UTC, but speeds decreased by roughly 50% aloft (Fig. 14c).

The balance of forces in the vertical averaged over the convective line portion of the 10–11 June MCS is compared with a similar force balance for a midlatitude squall line from Sanders and Emanuel (1977) in Fig. 15. Although both studies fail to accurately resolve the features within the convective line, some consistency in the results may indicate a systematic impact of squall lines on their environment. The pressure gradient and

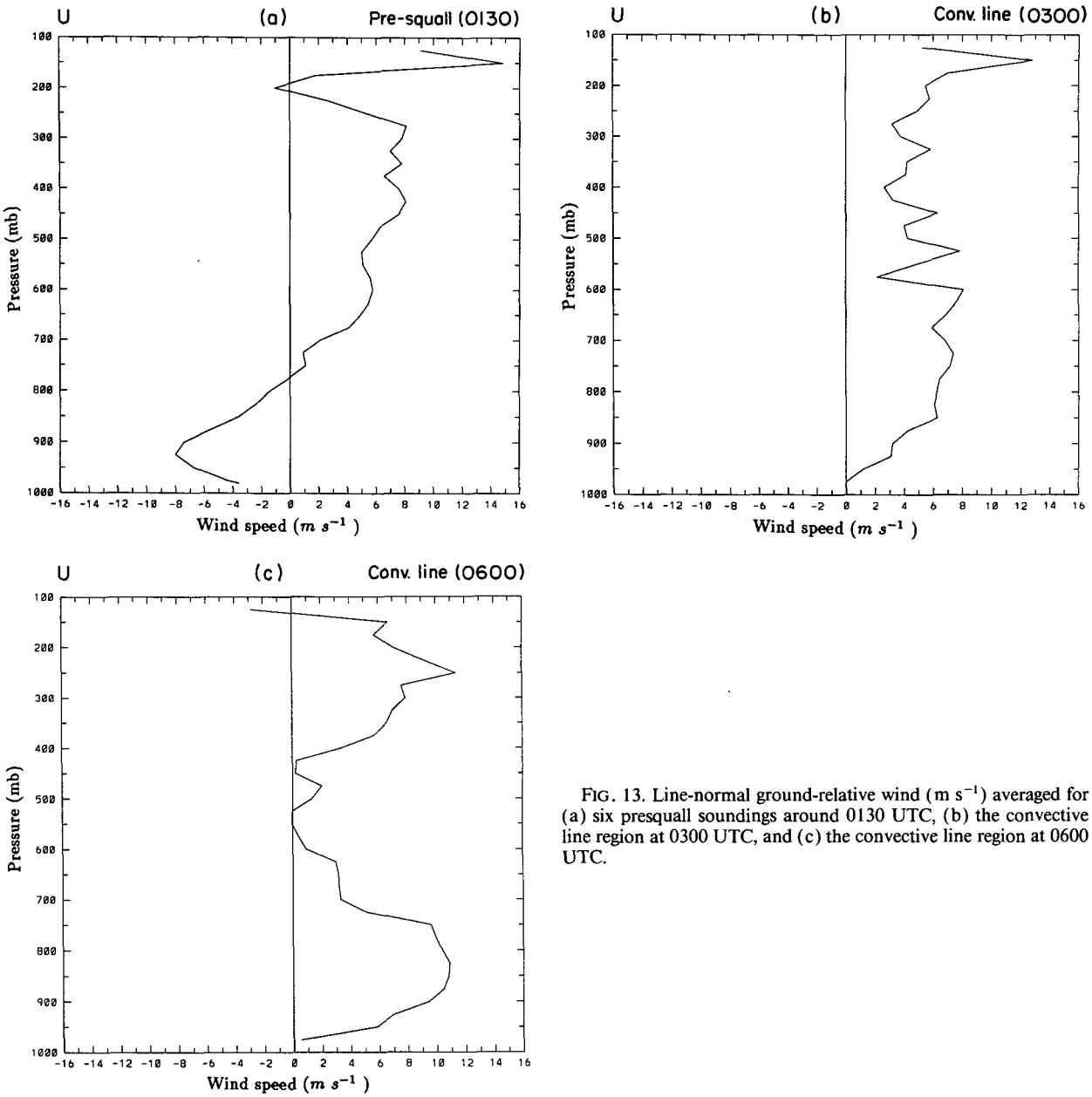

FIG. 13. Line-normal ground-relative wind (m s^{-1}) averaged for (a) six presquall soundings around 0130 UTC, (b) the convective line region at 0300 UTC, and (c) the convective line region at 0600 UTC.

Coriolis accelerations appear as rather smooth curves at both 0300 and 0600 UTC on 11 June (Figs. 15a,b). Below roughly 850 mb, the surface mesohigh led to rear-to-front pressure gradient acceleration at both times, although this acceleration was stronger and occurred over a slightly deeper layer at 0300 UTC (Fig. 15a). Front-to-rear acceleration dominated the pressure gradient force above this layer, although at 0600 UTC (Fig. 15b), some rear-to-front acceleration was occurring at high levels, ahead of the upper mesohigh. At least some of the observed temporal changes in the u profiles shown in Fig. 13 could be explained by the pressure gradient accelerations. The Coriolis force at 0300 and 0600 UTC was almost entirely from rear to front, increasing with height. The net effect of the pressure gradient and Coriolis forces acting alone would have resulted in a deep layer of front-to-rear acceleration, above 800 mb or so (and below 450 mb at 0600 UTC) (Figs. 15a,b). However, the actual total acceleration (local tendency minus advections) was rather variable with low-level rear-to-front acceleration, and only a few narrow bands of strong front-to-rear acceleration located around 425 and 625 mb at 0300 UTC (Fig. 15a), and 725 mb at 0600 UTC (Fig. 15b).

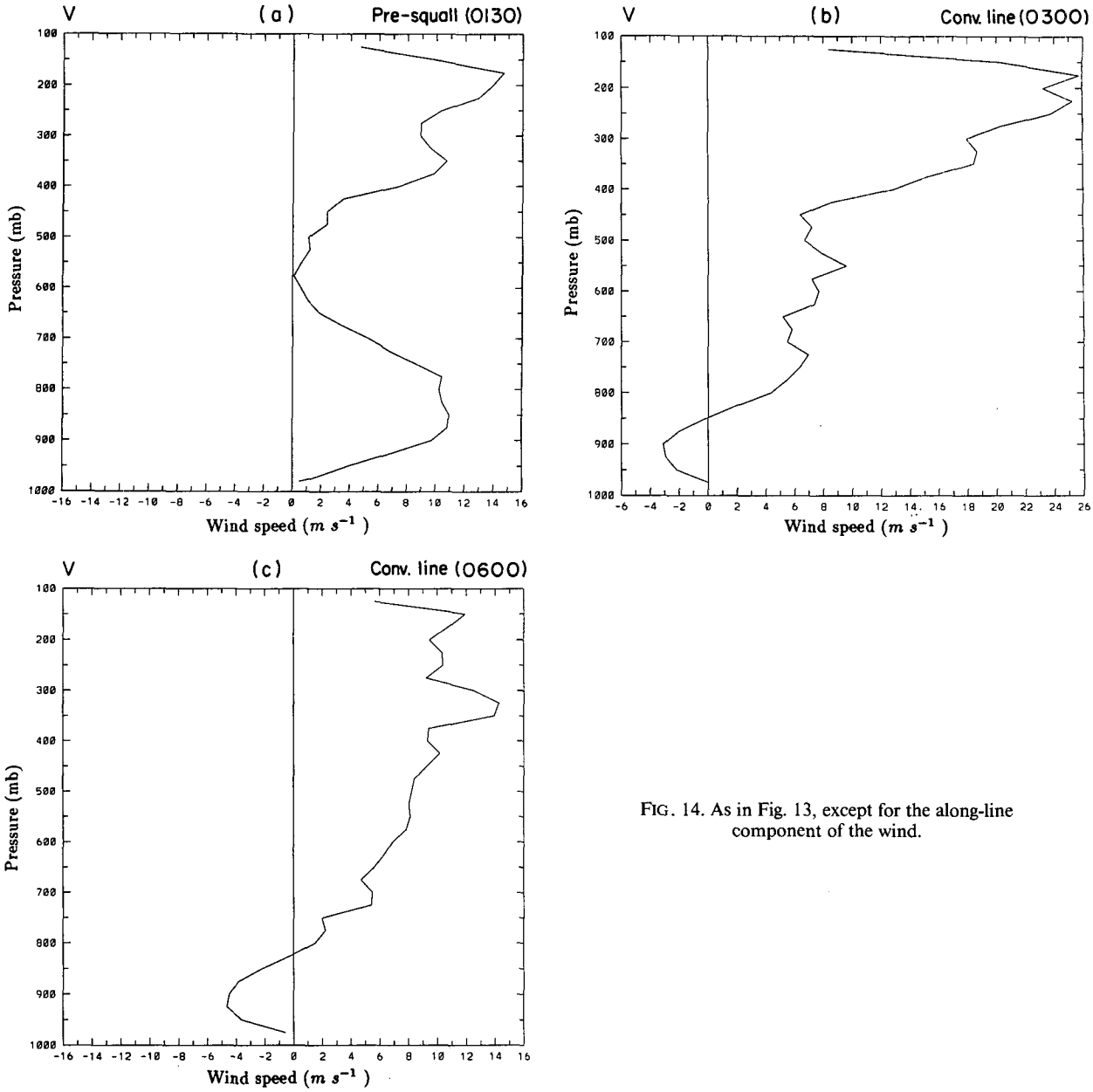

FIG. 14. As in Fig. 13, except for the along-line component of the wind.

Subgrid-scale momentum transport therefore appears to play an important role in accelerating the flow.

The results for 11 June generally agree well with those from Sanders and Emanuel (1977) (Fig. 15c), although different methods were used to obtain the pressure gradient and turbulent effects in both studies. The vertical profiles of the pressure gradient, Coriolis force, and turbulent stresses agree particularly well. In this study the pressure gradients were calculated directly from the rawinsonde height data (neglecting liquid water loading effects), and the turbulent stresses were solved for as a residual. Sanders and Emanuel used actual balloon measurements in their study to calculate the internal turbulent stresses, and solved for the pressure gradient as a residual. In general, they found that these pressure gradients were similar to those calculated from the reported rawinsonde heights, except at high levels (above 600 mb). They estimated liquid water loading from the difference between the height fields calculated using the two different methods. As in this case, Sanders and Emanuel found that $\bar{X}$ produced the strongest rear-to-front acceleration and was the primary acceleration opposing the pressure gradient at low to midlevels (Fig. 15c).

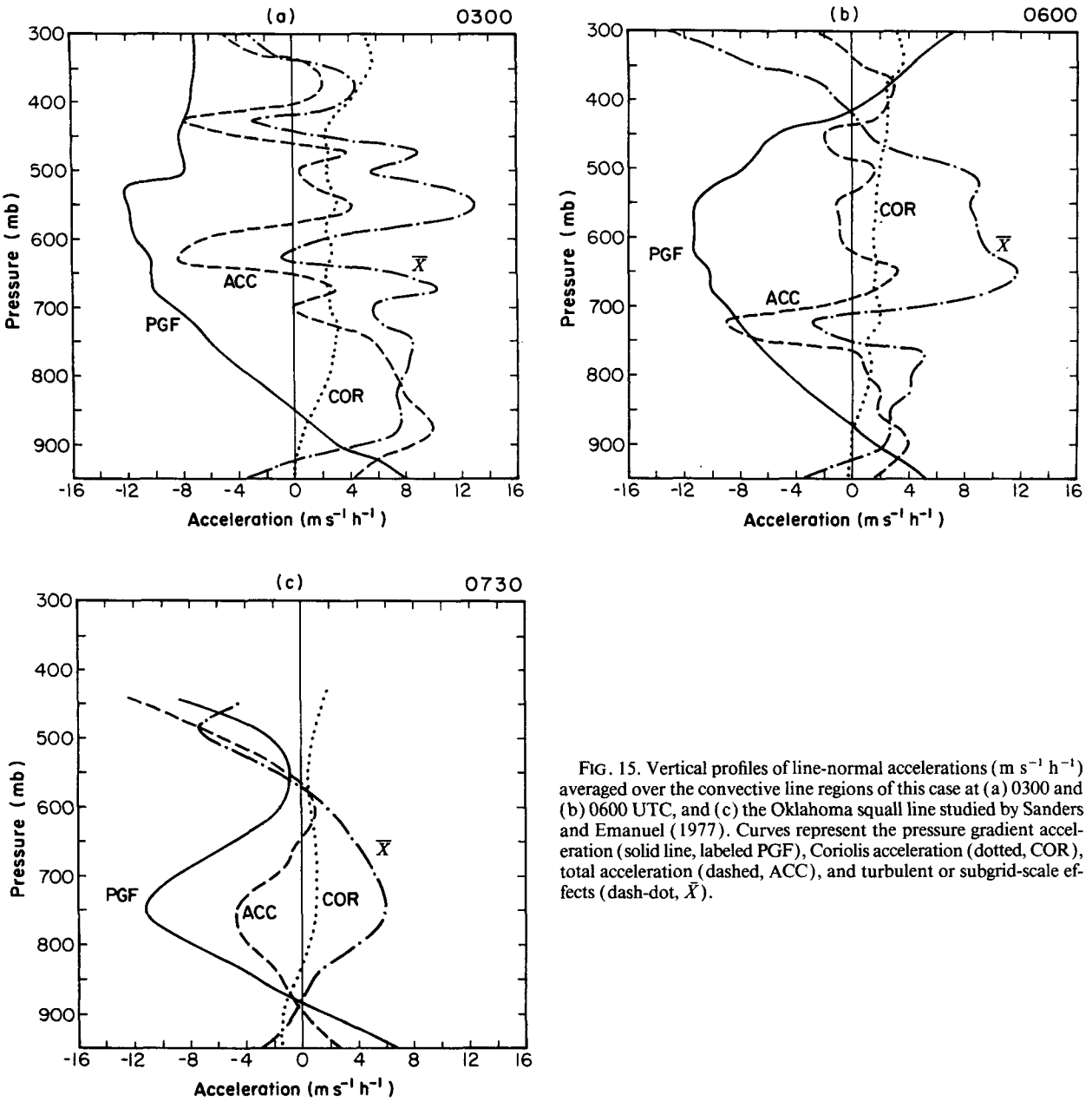

FIG. 15. Vertical profiles of line-normal accelerations (m s^{-1} h^{-1}) averaged over the convective line regions of this case at (a) 0300 and (b) 0600 UTC, and (c) the Oklahoma squall line studied by Sanders and Emanuel (1977). Curves represent the pressure gradient acceleration (solid line, labeled PGF), Coriolis acceleration (dotted, COR), total acceleration (dashed, ACC), and turbulent or subgrid-scale effects (dash-dot, $\bar{X}$).

The most significant difference between this squall line and the Sanders and Emanuel case appears to be in the profile of observed total acceleration. Sanders and Emanuel found midlevel front-to-rear acceleration dominating the vertical profile (Fig. 15c). On 11 June, front-to-rear accelerations were concentrated over relatively shallow layers (Figs. 15a,b), with accelerations from rear to front occurring throughout much of the low to middle troposphere in the convective line region. This may be a reflection of the dissipating state of the 11 June system. The Sanders and Emanuel squall line was at an earlier stage in its life cycle, when accelerations toward the rear at midlevels would be likely.

The individual components of the total acceleration (system-relative) averaged over the convective line are shown in Fig. 16. Local tendencies are generally small (less than 2 m s^{-1} h^{-1}), supporting the assumption of steady-state conditions for compositing. Some larger values around 450 mb at 0300 UTC may indicate that compositing could have introduced some error at that time. However, the system at 0300 UTC was still intense, and the stratiform and convective line regions

were not separated by a transition zone, so that aliasing was probably a more significant source of error than any compositing problems at that time. In the convective line at 0300 UTC (Fig. 16a) local tendencies were quite weak below 600 mb and somewhat stronger and negative aloft. Negative tendencies were also found at high levels in the convective line in the numerical simulation of Gao et al. (1990). They also found positive tendencies at low levels, which do not show up in our convective-line average, although weak positive tendencies did occur at low levels in the stratiform region at 0300 UTC (shown later). Their convective line profile was taken 40 km behind the leading edge of the system, and therefore was fairly close to the stratiform region, which might explain this difference. At 0600 UTC (Fig. 16b) the local tendencies were very weak, with generally negative values, except in the 400–650-mb layer.

Horizontal advection was strong from front to rear at low levels (as large as 9 m s^{-1} h^{-1} at 900 mb) at 0300 UTC (Fig. 16a) and weak and variable aloft (above ~600 mb). The intense negative acceleration at low levels was also found for this region at 0300 UTC by Gao et al. (1990). At high levels, they found large positive values 40 km behind the leading line, and more variable values at a distance of 80 km. The early termination of soundings within the convective system reduced the amount of data available for analyses at high levels at 0300 UTC, which may explain our variable profile above 550 mb, where Gao et al. found positive acceleration. At 0600 UTC (Fig. 16b) horizontal advections were much weaker, but still negative below ~650 mb. Vertical advections determined in this study, though relatively similar to those of the numerical simulation, are far more variable, possibly due to the presence of small-scale jets in the system, or inaccurate rawinsonde wind data in certain layers. Gao et al. (1990) found that vertical advections tended to offset horizontal advections in the convective system. This result is not readily apparent from the sounding data in the convective line. There is more evidence of such a balance in the stratiform region (to be shown later).

Vertical profiles for the balance of forces in the stratiform region at 0300, 0600, and 0730 UTC are shown in Fig. 17. At 0300 UTC (Fig. 17a) rearward pressure gradient acceleration was acting at all levels. The Coriolis force imposed rearward acceleration below 800 mb, but rear-to-front acceleration above that level. Observed total accelerations were weak from rear to front below 750 mb, with front-to-rear acceleration at higher levels, with the exception of an ~50-mb-deep layer centered at ~550 mb. This rearward acceleration aloft helped to increase the rate at which hydrometeors were transported rearward within the stratiform anvil cloud, resulting in a substantial broadening of the stratiform rain region around this time. The variability

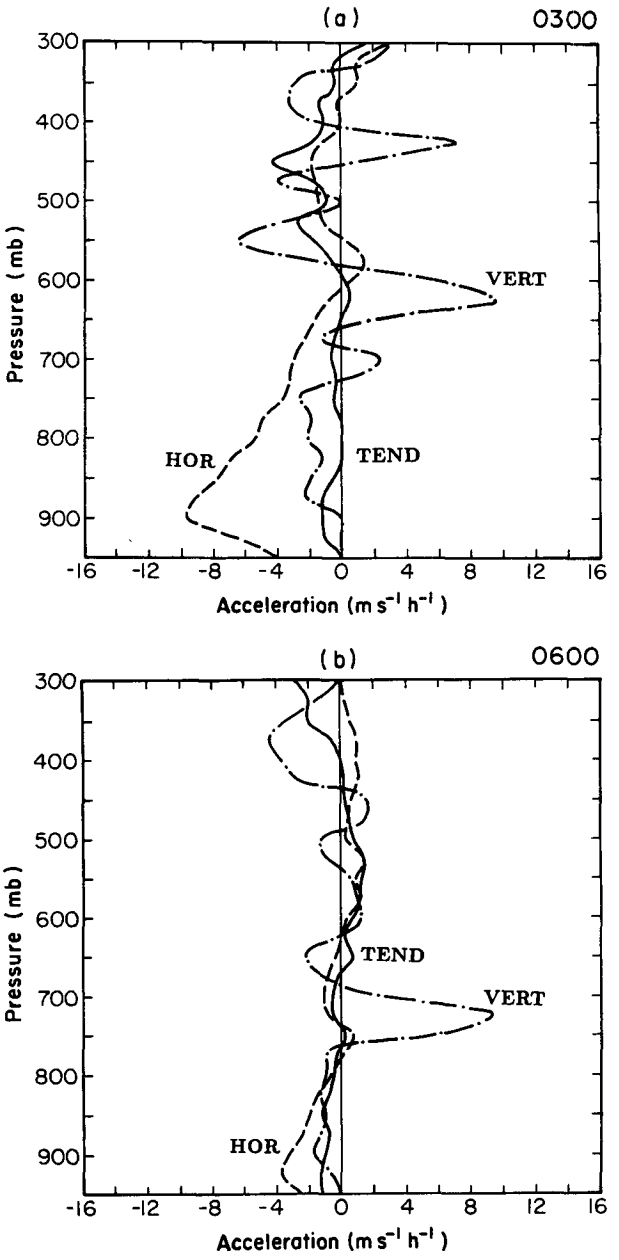

FIG. 16. Vertical profiles of components of the line-normal total acceleration averaged over the convective line region at (a) 0300 and (b) 0600 UTC (in units of m s^{-1} h^{-1}). Local tendency ($D\bar{u}/Dt$) is shown by solid line (TEND), horizontal advection ($-\bar{u}\partial\bar{u}/\partial x - \bar{v}\partial\bar{u}/\partial y$) a dashed line (HOR), and vertical advection ($-\bar{\omega}\partial\bar{u}/\partial p$) with a dashed-dotted line (VERT).

of the acceleration profile at 0300 UTC may in part be a result of aliasing of the wind fields and vertical motions from the intense convective line into the stratiform region. It is also possible that some of the extrema in the observed acceleration profile were due to subgrid-scale momentum sources and sinks from weak convective elements within the stratiform region.

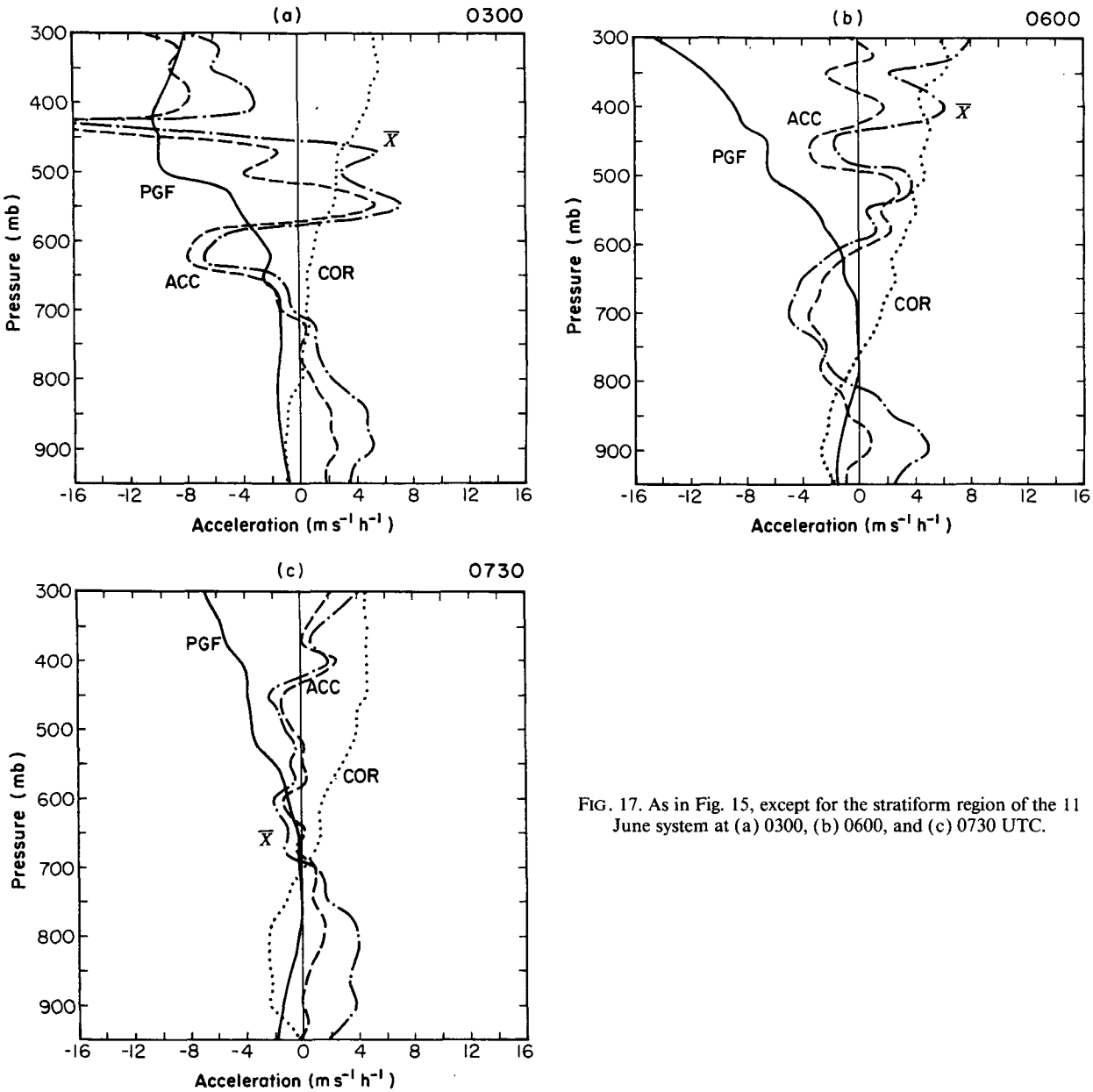

FIG. 17. As in Fig. 15, except for the stratiform region of the 11 June system at (a) 0300, (b) 0600, and (c) 0730 UTC.

At 0600 UTC (Fig. 17b) the pressure gradient force continued to generally be directed rearward, except in the 700–800-mb layer where it was nearly zero. This layer is a region where some rear-to-front acceleration was occurring at the back of the stratiform region (Fig. 7b) due to the midlevel mesolow centered within the stratiform region. The Coriolis force at 0600 UTC resembled that at 0300 UTC, although the layer of negative acceleration now extended up to 750 mb. Extreme values of the observed and subgrid-scale accelerations weakened from 0300 to 0600 UTC, possibly a result of weakening convection and less aliasing from the convective line region as the system broadened. At 0730 UTC (Fig. 17c), this weakening continued, and the Coriolis and pressure gradient forces were nearly in balance above 600 mb, supporting the observations of minimal acceleration and subgrid-scale effects. A layer of near-zero pressure gradient acceleration force continued to exist in the 650–800-mb layer, but otherwise the pressure gradient continued to be directed rearward.

The individual components of the total acceleration (system relative) averaged over the stratiform region can be seen in Fig. 18. Local tendencies were somewhat larger than in the convective line (Figs. 16a and 16b),

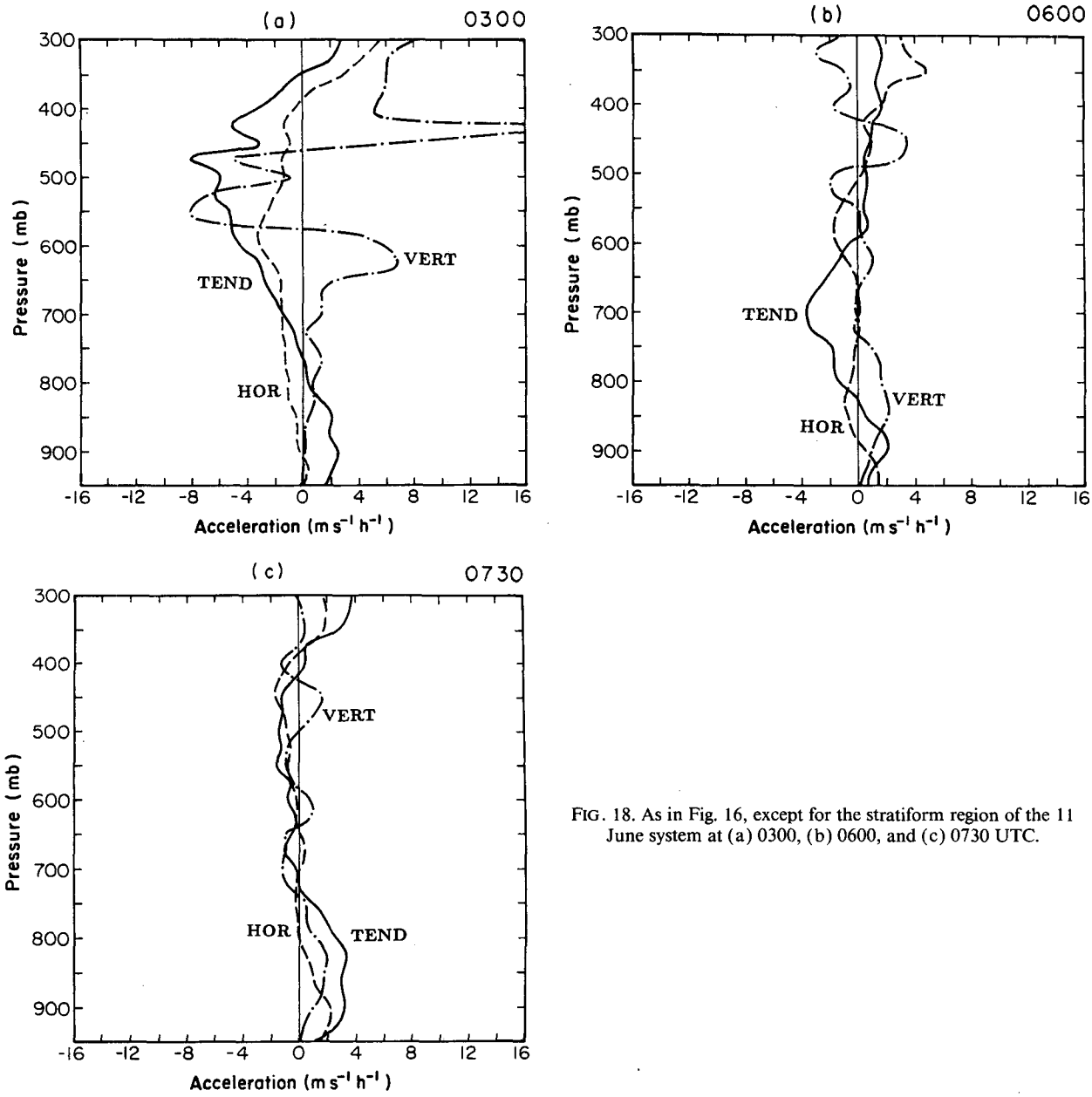

FIG. 18. As in Fig. 16, except for the stratiform region of the 11 June system at (a) 0300, (b) 0600, and (c) 0730 UTC.

but still rather small, except at 0300 UTC. Negative tendencies were greatest around 500 mb at 0300 UTC (Fig. 18a), and at 700 mb at 0600 UTC (Fig. 18b). At 0300 UTC positive tendencies were confined to layers below 750 mb, with significant negative tendencies elsewhere. At 0600 and 0730 UTC (Figs. 18b and 18c) tendencies remained positive at low levels, but generally were weak and variable throughout the troposphere. Horizontal advection was weak at all three times. It was generally positive at 0300 UTC and variable later. At 0300 UTC (Fig. 18a) strong vertical advection was occurring above 650 mb, with the strongest (from rear to front) at 450 mb. This may be an indication of some intense convective cells within the young stratiform anvil at that time. Some of the intensity of the advection may also be due to aliasing problems at 0300 UTC. At 0600 UTC (Fig. 18b) vertical advection weakened significantly as the intense convection dissipated. At 0730 UTC (Fig. 18c) vertical advection continued to weaken and was now less significant than horizontal advection. At 0300 UTC (Fig. 18a), the horizontal advection was generally opposing the vertical advection below 600 mb (as in Gao et al. 1990). At 0600 UTC (Fig. 18b) this opposition was occurring in several layers, and

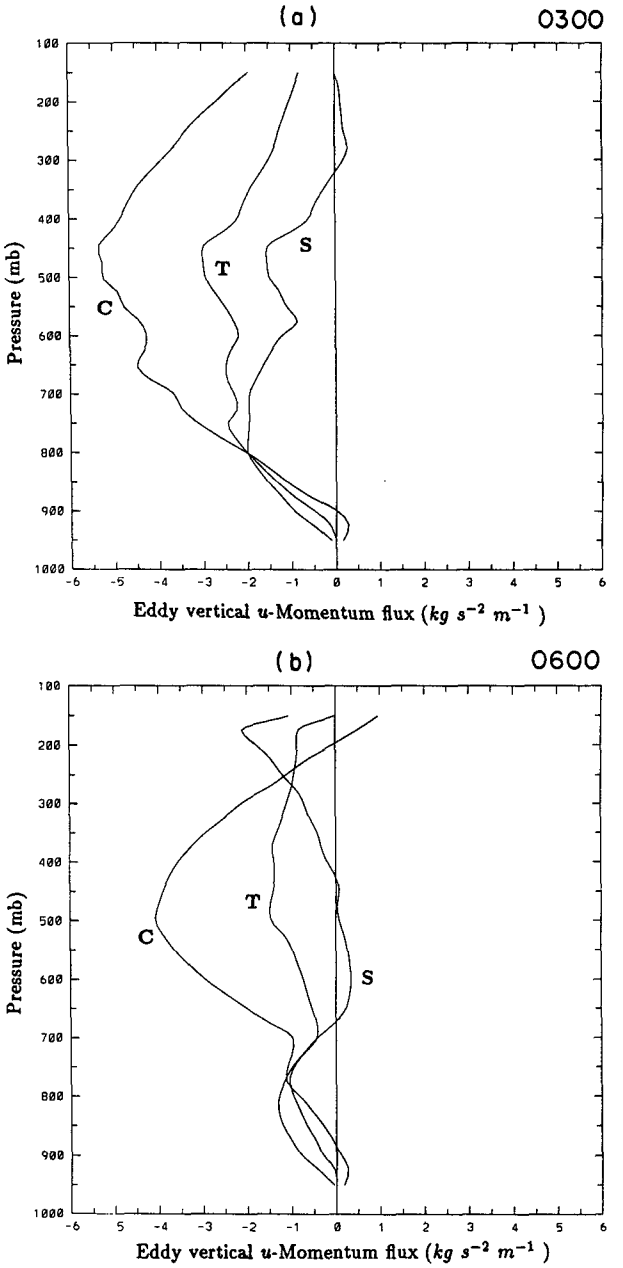

FIG. 19. Vertical profiles of the eddy vertical u-momentum flux (kg m^{-1} s^{-2}) at (a) 0300 and (b) 0600 UTC, averaged over the convective line region (curve C), stratiform region (curve S), and entire system (curve T).

weak evidence of it appeared at 0730 UTC (Fig. 18c). Although a balance between the horizontal and vertical advections was evidenced more in the stratiform region than in the convective line (Fig. 16), in neither region was it very definitive.

The vertical component of the eddy u-momentum flux ($\rho\overline{w'u'}$) averaged over the convective line and stratiform regions and the entire system at 0300 and 0600 UTC can be seen in Fig. 19. This flux was computed by integrating the last term (the vertical divergence of the vertical eddy momentum flux) in (1) from the surface to 125 mb, converting ω to w, and neglecting horizontal eddy transports. Although the structure of this squall line may have led to some contribution from horizontal eddy effects, they cannot be measured from sounding data, and to be consistent with other rawinsonde-based studies, it was assumed that the horizontal eddy fluxes would be smaller than the vertical eddy fluxes. Within the convective line, the flux was primarily negative at all levels at 0300 UTC (Fig. 19a), and everywhere below 200 mb at 0600 UTC (Fig. 19b). These profiles resemble those for the numerical simulation of this case by Gao et al. (1990), and other midlatitude and tropical cases by LeMone (1983), Smull and Houze (1987a), and Lafore et al. (1988). In spite of the neglect of horizontal eddy transports and the fluxes being computed from the integration of a residual term, ($\bar{X}$), the magnitudes and shape of the curves are close to those found in the Gao et al. simulation, and $\bar{X}$ itself agrees with the magnitudes found in the Doppler radar study of this case by Smull and Houze (1987a). Peak negative fluxes occurred at 450 mb at 0300 UTC (Fig. 19a) and 500 mb at 0600 UTC (Fig. 19b).

Negative values of $\rho\overline{w'u'}$ indicate that front-to-rear flow was ascending within the convective line. It was shown earlier (Fig. 13a) that there was positive shear of the presquall winds (as opposed to negative shear in the LeMone 1983 case) so that negative $\overline{w'u'}$ would be expected from mixing-length theory. However, because the flux was computed from a residual term that was determined using wind and height data at the three specific budget times (0300, 0600, and 0730 UTC), it was felt that only the wind profiles taken at those specific times should be used for comparisons with the flux profiles to determine whether transport was down- or countergradient. At 0300 UTC, the wind shear in the convective line had become weak and variable (Fig. 13b), and the computed transport would not be expected using normal downgradient arguments. By 0600 UTC the wind and flux profiles indicated that the momentum transport in the convective line was definitely countergradient below 500 mb (compare Fig. 13c and 19b). As in LeMone (1983), this countergradient momentum flux can be attributed to the midlevel mesolow behind the leading convective line producing strong front-to-rear flow.

This type of evolution of the wind shear and its relation to the momentum transport have been described by Matejka and LeMone (1990) for another case. For this case, the eddy transport would accelerate rear-to-front flow below midlevels, and front-to-rear flow aloft. These accelerations would act to increase the weak negative shear at 0300 UTC (see Fig. 13b), but have mixed effects at the later times. The vertical eddy U-

momentum flux within the stratiform region was still generally negative at both 0300 and 0600 UTC, due to ascending front-to-rear flow in the anvil and descending rear-to-front flow below. The negative flux was, however, much weaker than in the convective line, with a midlevel region of positive flux at 0600 UTC. This could be associated with the lowest layers of front-to-rear flow above the rear-inflow jet (Fig. 2b), descending (Fig. 4b) due to cooling from evaporation, sublimation, and melting.

5. Momentum budget of the along-line flow

Although the components of the u-momentum budget of the 10–11 June squall line varied little in the along-line direction, the components of the v-momentum budget varied markedly in a rather chaotic pattern, so that averaging of individual components along the 50-km-wide strips used in the vertical cross sections shown earlier seemed unrepresentative of the general pattern. In addition, any particular vertical cross section would not be representative of the system as a whole. Therefore, only brief discussion will be given to the along-line momentum budget of the 10–11 June squall line.

Vertical profiles of the forces acting on the along-line component of the wind averaged over the larger convective line and stratiform regions of the system can be seen in Figs. 20 and 21, respectively. In general, the ambient pressure gradient controlled accelerations along the convective line, with weak southwesterly (positive) acceleration dominating at both 0300 and 0600 UTC (Figs. 20a,b). From horizontal cross sections, the midlevel mesolow (Fig. 5) could be seen influencing the pressure gradient accelerations, with northeasterly acceleration at the north end of the system (figure not shown). At high levels, an intense mesohigh centered in the southern part of the line resulted in strong southwesterly acceleration, exceeding 20 m s^{-1} h^{-1} at some points at 0600 UTC, over the northern two-thirds of the squall line (figure not shown). Gao et al. (1990) have shown that during intensification of the system (0000 UTC) this acceleration exceeded 40 m s^{-1} h^{-1}. They have also shown, however, that advections tended to cancel this generation of momentum by the pressure gradient force. Some northeasterly pressure gradient acceleration occurred at high levels over the southern end of the system. Coriolis accelerations were from the northeast but were quite weak in the convective line. The observed acceleration and the subgrid-scale effects were highly variable in the vertical with northeasterly acceleration dominating the low levels and southwesterly acceleration common at high levels. The southwesterly acceleration was strongest around 400 mb, with peak values weakening from over 12 m s^{-1} h^{-1} at 0300 UTC (Fig. 20a) to 7 m s^{-1} h^{-1} at 0600 UTC (Fig. 20b).

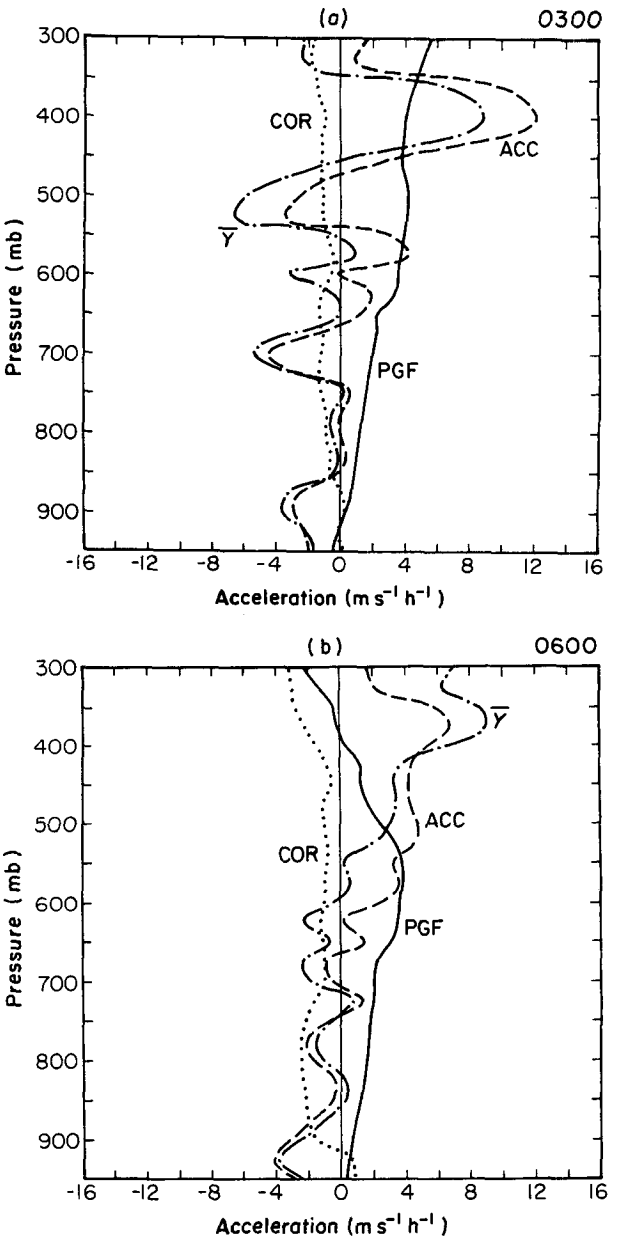

FIG. 20. As in Fig. 15, except for along-line accelerations averaged over the convective line of the 11 June system at (a) 0300 and (b) 0600 UTC (with subgrid-scale effects curve $\bar{Y}$).

In the stratiform region (Fig. 21), the ambient pressure gradient also dominated the accelerations with weak positive (southwesterly) values at all levels. Coriolis accelerations were stronger in the stratiform region than in the convective line and were the dominant northeasterly acceleration in this region. The observed acceleration (curve ACC) and the residual $\bar{Y}$ were generally southwesterly at 0300 UTC (Fig. 21a) but the observed acceleration switched to northeasterly below ~650 mb at 0600 (Fig. 21b) and both became north-

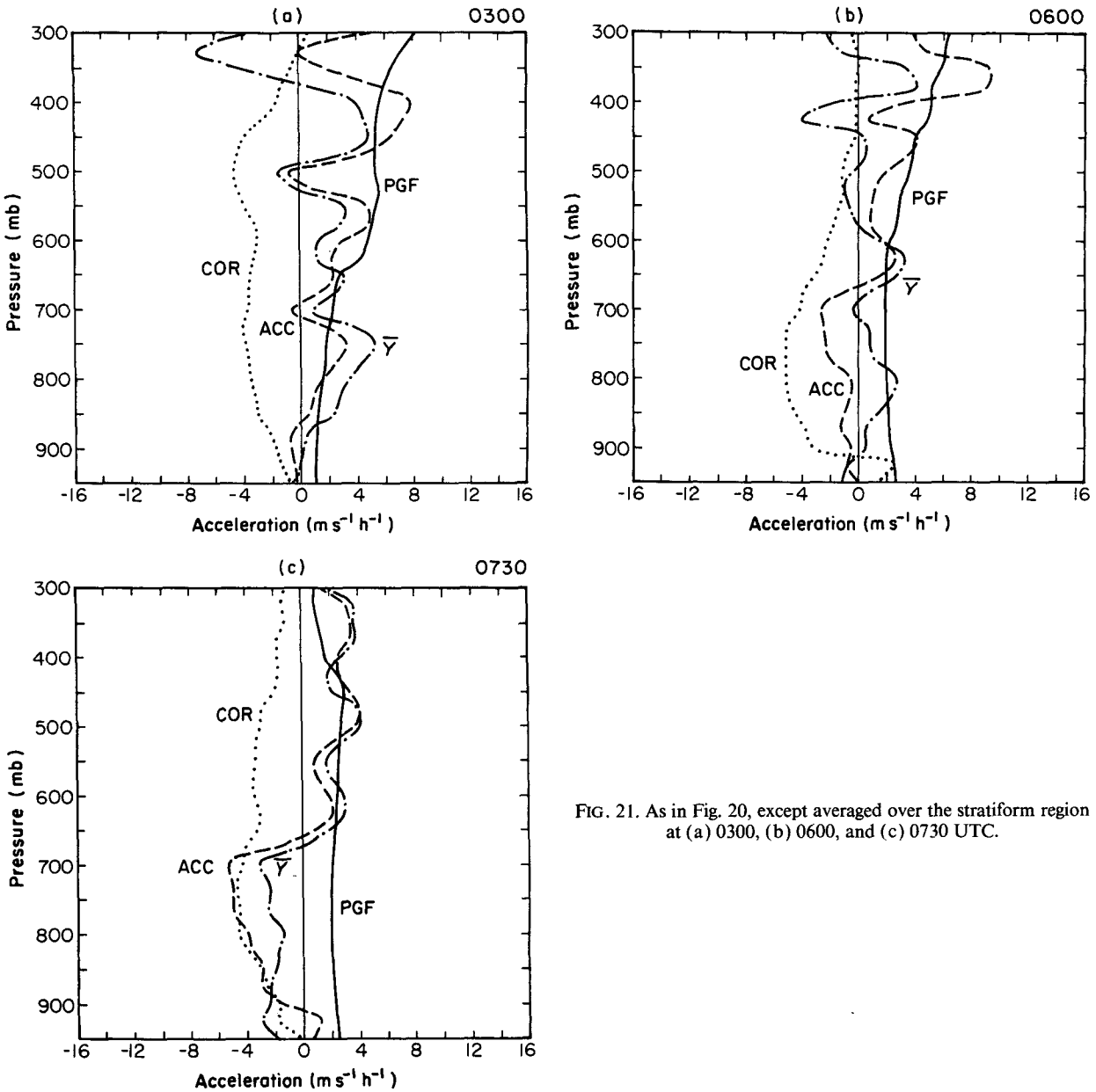

FIG. 21. As in Fig. 20, except averaged over the stratiform region at (a) 0300, (b) 0600, and (c) 0730 UTC.

easterly at low levels by 0730 UTC (Fig. 21c). Strong northeasterly acceleration occurred just behind the midlevel mesolow (figure not shown), possibly indicating the intensification of a cyclonic circulation. Overall, the diagnosed accelerations implied an increase of the positive v vertical wind shear below 300 mb throughout the system at 0300 and 0600 UTC (cf. Fig. 14b,c). The vertical shear of the along-line winds did increase below this level through 0300 UTC, and then remained relatively constant through 0600 UTC (Fig. 14).

The vertical component of the eddy v-momentum flux ($\overline{\rho w'v'}$) is averaged over the convective line and stratiform regions, and the entire system at 0300 and 0600 UTC can be seen in Fig. 22. As in the computation of $\overline{\rho w'u'}$, the horizontal eddy term was neglected in the integrations. As found in most budgets of fast-moving squall lines (LeMone et al. 1984; Smull and Houze 1987a; Lafore et al. 1988) the along-line momentum flux in the convective line was much smaller than the u-momentum flux (Fig. 19). The two fluxes were more nearly equal within the stratiform region. Within the convective line, the flux was strictly positive at 0300 UTC (Fig. 22a) and positive below 400 mb at 0600 UTC (Fig. 22b), with weak maxima at midlevels at both times. The eddy momentum flux in the con-

vective line therefore was generally countergradient (cf. Figs. 14b,c), and the vertical profile indicates northeasterly acceleration at low levels with southwesterly acceleration aloft. The changes between the presquall and 0300 UTC convective-line v profiles (Figs. 14a and 14b) support this increase in shear. The shear did not increase between 0300 and 0600 UTC (Figs. 14b and 14c), and in fact decreased above 400 mb, which may indicate that the data at high levels at 0600 UTC were adversely affected by an updraft-core sounding, leading to erroneous values of the momentum flux. The greatest negative fluxes occurred within the stratiform region (with the exception of high levels at 0600 UTC, which also may have been adversely affected by the updraft core sounding). For the entire system, though, the v-momentum flux tended to be weakly negative with magnitudes at all levels less than 1 kg m^{-1} s^{-2}. This weak negative flux for the entire system would mean a downgradient transport of along-line momentum, agreeing with results for other convective systems (LeMone 1983; Gao et al. 1990).

The countergradient transport observed in the convective line may be a result of the chosen domain and asymmetries in the along-line pressure field. Convective line averages were determined from data points located within the region of intense radar echo observed from the Wichita and Oklahoma City radars (GJ, Fig. 1), and therefore, intense convective cells at the north and south ends of the line may not have been contained within the domain. However, it does appear to us that the v and v-flux profiles shown in the Gao et al. (1990) numerical simulation of this case, taken over the northern half of the entire system, also indicate some countergradient transport of along-line momentum, and an increase in vertical shear. The countergradient transport may be due, in part, to the location of the mesolow within the northern part of the squall line (see Fig. 5). If it is the midlevel mesolow that contributes to countergradient momentum fluxes in squall lines (LeMone 1983), then it is perhaps not surprising that for squall lines such as this one that exhibit pronounced along-line asymmetries in the pressure field, localized countergradient fluxes can also be detected in the along-line direction. If these results are correct, the 10–11 June squall line not only transported line-normal momentum countergradient (similar to observations from many other cases), but also along-line momentum, a result distinctly different from other cases.

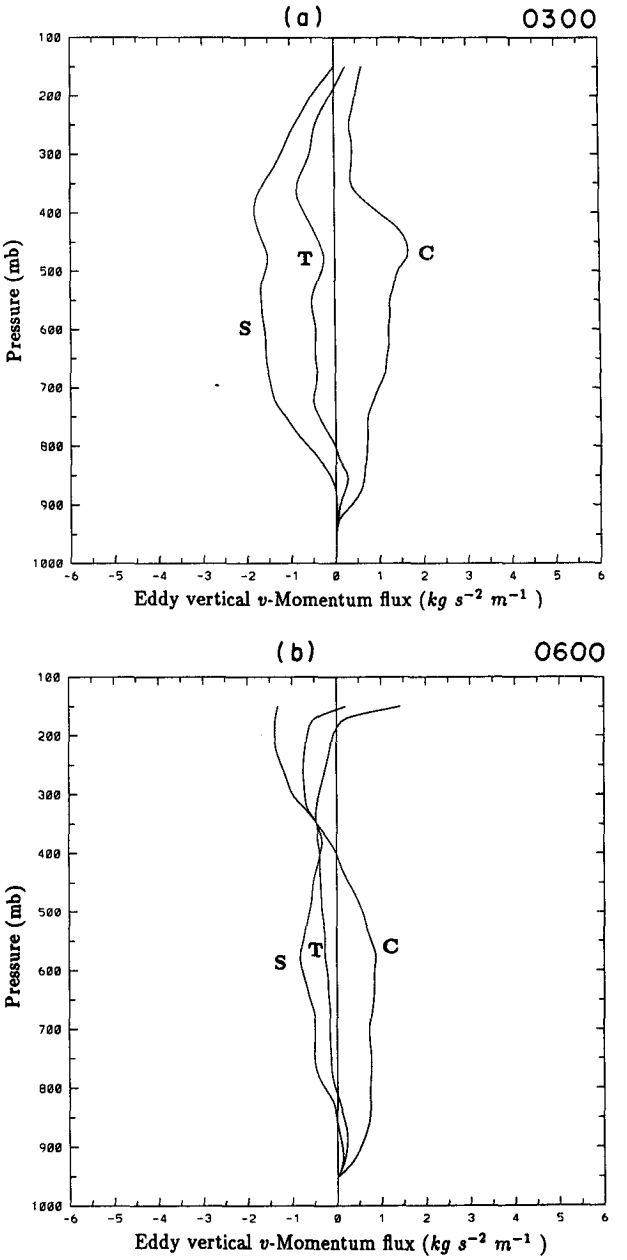

FIG. 22. As in Fig. 19, except for the eddy vertical v-momentum flux.

6. Conclusions and discussion

In this study, rawinsonde data from the 10–11 June PRE-STORM squall line case have been used to examine the evolution of line-normal and along-line momentum budgets during the mature through dissipating stages of this intense midlatitude MCS. Momentum budgets were done in a system-relative reference frame so that comparison could easily be made with results of the numerical simulation of this case by Gao et al. (1990). Composites were made using soundings taken over 3-hour time intervals as in Gallus and Johnson (1991). Low-level reflectivity data were used to partition the system into convective line and stratiform areas, and comparisons were made between the budgets of the different regions.

A rather intense midlevel mesolow has been documented, and this mesolow causes rear-to-front acceleration in the vicinity of the observed rear-inflow jet. In addition, the mesolow along with a pressure minimum sloping rearward with height leads to strong front-to-rear pressure gradient acceleration throughout a large portion of the convective system. Local momentum tendencies, horizontal advections, and particularly vertical advections throughout the squall line weakened during the dissipating stages of the system. Convective-scale effects, solved for as a residual, appear to primarily cause rear-to-front acceleration at low levels, and front-to-rear acceleration aloft. Rather strong rearward subgrid-scale acceleration occurring near the axis of the rear-inflow jet may be evidence of mixing taking place within the zone of intense shear between this jet and the strong front-to-rear jet.

Averages taken over the convective-line portion of the squall line show some similarity with results obtained for another midlatitude system (Sanders and Emanuel 1977), with pressure gradient forces being primarily responsible for rearward acceleration, and subgrid-scale effects primarily opposing this acceleration. In the stratiform region, observed total accelerations and subgrid-scale effects became negligible during dissipation, so that a balance roughly existed between the pressure gradient and Coriolis forces.

Vertical integration of the subgrid-scale term from the surface to 125 mb (neglecting horizontal eddy fluxes) showed that the line-normal momentum flux was generally negative within the system (similar to LeMone 1983), and the divergence of this flux resulted in rear-to-front acceleration at low levels and front-to-rear acceleration aloft. Negative flux would be expected from downgradient arguments applied to presquall soundings, but it is shown that the wind shear reversed under the influence of the convective line, so that the momentum flux was actually countergradient in the squall line, agreeing with previous case studies.

The momentum budget of the along-line flow was found to be less organized than that of the line-normal flow. The integrated subgrid-scale term showed weak positive momentum flux in the convective line region, with weak negative fluxes in the stratiform region, and for the system as a whole. The positive flux in the convective line agrees with results found in other cases and the numerical simulation of this system (Gao et al. 1990). However, positive shear of the along-line component of the wind dominated by the time of these budgets, so that the positive flux within the convective line would indicate countergradient transport, contrary to the downgradient transport usually calculated for the along-line flow in other convective systems (LeMone 1983). This result may be due to the presence of the midlevel mesolow within the northern part of the squall-line system. It may also be influenced by our domain, which was unable to include the entire convective line, since the north and south ends of the system were outside the region of adequate PRE-STORM rawinsonde data. Another problem with the data, as in Gallus and Johnson (1991), was the early termination of soundings that ascended within the convective system. The early termination prohibits as accurate an analysis of data at high levels as there is at lower levels. These problems should be addressed in the planning of future mesoscale field programs.

Acknowledgments. We would like to thank Dr. Margaret LeMone for her helpful discussions on this subject, James Bresch for his assistance with the computer programming, and Gail Cordova for preparation of the final manuscript. The helpful comments of Prof. Da-Lin Zhang and two anonymous reviewers were appreciated. This research was supported by the National Science Foundation Grants ATM-8711649 and ATM-9013112, and a National Science Foundation Graduate Fellowship.

REFERENCES

Augustine, J. A., and E. J. Zipser, 1987: The use of wind profilers in a mesoscale experiment. *Bull. Amer. Meteor. Soc.*, **68**, 4–17.

Barnes, S. L., 1964: A technique for maximizing details in numerical weather map analysis. *J. Appl. Meteor.*, **3**, 396–409.

Bluestein, H. B., and M. H. Jain, 1985: Formation of mesoscale lines of precipitation: Severe squall lines in Oklahoma during the spring. *J. Atmos. Sci.*, **42**, 1711–1731.

Brown, J. M., 1979: Mesoscale unsaturated downdrafts driven by rainfall evaporation: A numerical study. *J. Atmos. Sci.*, **36**, 313–338.

Fankhauser, J. C., 1974: The derivation of consistent fields of wind and geopotential height from mesoscale rawinsonde data. *J. Appl. Meteor.*, **13**, 637–646.

Fovell, R. G., 1991: Influence of the Coriolis force on two-dimensional model storms. *Mon. Wea. Rev.*, **119**, 606–630.

Fritsch, J. M., and R. A. Maddox, 1981: Convectively driven mesoscale weather systems aloft. Part I: Observations. *J. Appl. Meteor.*, **20**, 9–19.

——, and J. M. Brown, 1982: On the generation of convectively driven mesohighs aloft. *Mon. Wea. Rev.*, **110**, 1554–1563.

Fujita, T. T., 1955: Results of detailed synoptic studies of squall lines. *Tellus*, **7**, 405–436.

Gallus, W. A., Jr., and R. H. Johnson, 1991: Heat and moisture budgets of an intense midlatitude squall line. *J. Atmos. Sci.*, **48**, 122–146.

Gao, K., D.-L. Zhang, M. W. Moncrieff, and H.-R. Cho, 1990: Mesoscale momentum budget in a midlatitude squall line: A numerical case study. *Mon. Wea. Rev.*, **118**, 1011–1028.

Houze, R. A., Jr., S. A. Rutledge, M. I. Biggerstaff, and B. F. Smull, 1989: Interpretation of Doppler weather radar displays of midlatitude mesoscale convective systems. *Bull. Amer. Meteor. Soc.*, **70**, 608–619.

Johnson, R. H., and P. J. Hamilton, 1988: The relationship of surface pressure features to the precipitation and air flow structure of an intense midlatitude squall line. *Mon. Wea. Rev.*, **116**, 1444–1472.

——, W. A. Gallus, Jr., and M. W. Vescio, 1990: Near tropopause vertical motion within the trailing stratiform regions of squall lines. *J. Atmos. Sci.*, **47**, 2200–2210.

LaFore, J.-P., and M. W. Moncrieff, 1989: A numerical investigation of the organization and interaction of the convective and stratiform regions of tropical squall lines. *J. Atmos. Sci.*, **46**, 521–524.

——, J.-L. Redelsperger, and G. Jaubert, 1988: Comparison between

a three-dimensional simulation and Doppler radar data of a tropical squall line: transports of mass, momentum, heat and moisture. *J. Atmos. Sci.*, **45**, 3483–3500.

Leary, C. A., and R. A. Houze, Jr., 1979: The structure and evolution of convection in a tropical cloud cluster. *J. Atmos. Sci.*, **36**, 437–457.

LeMone, M. A., 1983: Momentum transport by a line of cumulonimbus. *J. Atmos. Sci.*, **40**, 1815–1834.

——, G. M. Barnes, and E. J. Zipser, 1984: Momentum fluxes by lines of cumulonimbus over the tropical oceans. *J. Atmos. Sci.*, **41**, 1914–1932.

Maddox, R. A., D. J. Perkey, and J. M. Fritsch, 1981: Evolution of upper tropospheric features during the development of a mesoscale convective complex. *J. Atmos. Sci.*, **38**, 1664–1674.

Matejka, T., 1989: Pressure and buoyancy forces and tendencies in a squall line and their relation to its evolution. Preprints, *24th Conf. on Radar Meteorology.* Tallahassee, Amer. Meteor. Soc., 478–481.

——, and M. A. LeMone, 1990: The generation and redistribution of momentum in a squall line. Preprints, *Fourth Conf. on Mesoscale Processes.* Boulder, Colorado, Amer. Meteor. Soc., 196–197.

Menard, R. D., and J. M. Fritsch, 1989: A mesoscale convective complex-generated inertially stable warm core vortex. *Mon. Wea. Rev.*, **117**, 1237–1261.

Moncrieff, M. W., 1981: A theory of organized steady convection and its transport properties. *Quart. J. Roy. Meteor. Soc.*, **107**, 29–50.

O'Brien, J. J., 1970: Alternative solutions to the classical vertical velocity problem. *J. Appl. Meteor.*, **9**, 197–203.

Ogura, Y., and M. T. Liou, 1980: The structure of a midlatitude squall line. *J. Atmos. Sci.*, **37**, 553–567.

Rutledge, S. A., R. A. Houze, Jr., M. I. Biggerstaff, and T. Matejka, 1988: The Oklahoma–Kansas mesoscale convective system of 10–11 June 1985: Precipitation structure and single-Doppler radar analysis. *Mon. Wea. Rev.*, **116**, 1409–1430.

Sanders, F., and K. Emanuel, 1977: The momentum budget and temporal evolution of a mesoscale convective system. *J. Atmos. Sci.*, **34**, 322–330.

Smull, B. F., and R. A. Houze, Jr., 1985: A midlatitude squall line with a trailing region of stratiform rain: radar and satellite observations. *Mon. Wea. Rev.*, **113**, 117–133.

——, and ——, 1987a: Dual-Doppler radar analysis of a midlatitude squall line with a trailing region of stratiform rain. *J. Atmos. Sci.*, **44**, 2128–2148.

——, and ——, 1987b: Rear inflow in squall lines with trailing stratiform precipitation. *Mon. Wea. Rev.*, **115**, 2869–2889.

Stevens, D. E., 1979: Vorticity, momentum and divergence budgets of synoptic-scale wave disturbances in the tropical Eastern Atlantic. *Mon. Wea. Rev.*, **107**, 535–550.

Wetzel, P. J., W. R. Cotton, and R. L. McAnelly, 1983: A long-lived mesoscale convective complex. *Mon. Wea. Rev.*, **111**, 1919–1937.

Zhang, D.-L., and K. Gao, 1989: Numerical simulation of an intense squall line during 10–11 June 1985 PRE-STORM. Part II: Rear inflow, surface wake lows and stratiform precipitation. *Mon. Wea. Rev.*, **117**, 2067–2094.

——, ——, and D. B. Parsons, 1989: Numerical simulation of an intense squall line during 10–11 June 1985 PRE-STORM. Part I: Model verification. *Mon. Wea. Rev.*, **117**, 960–994.